PCCP

ROYAL SOCIETY OF CHEMISTRY

PAPER

View Article Online
View Journal | View Issue

Check for updates

Cite this: *Phys. Chem. Chem. Phys.*, 2022, **24**, 6699

Cu^{2+}-Induced self-assembly and amyloid formation of a cyclic D,L-α-peptide: structure and function†

Daniel Klose, ‡[a] Sahithya Phani Babu Vemulapalli, ‡[bc] Michal Richman,‡[d] Safra Rudnick,[de] Vered Aisha,[d] Meital Abayev,[d] Marina Chemerovski,[d] Meital Shviro,[de] David Zitoun, [de] Katharina Majer,[a] Nino Wili, [a] Gil Goobes, [d] Christian Griesinger, *[b] Gunnar Jeschke*[a] and Shai Rahimipour *[d]

In a wide spectrum of neurodegenerative diseases, self-assembly of pathogenic proteins to cytotoxic intermediates is accelerated by the presence of metal ions such as Cu^{2+}. Only low concentrations of these early transient oligomeric intermediates are present in a mixture of species during fibril formation, and hence information on the extent of structuring of these oligomers is still largely unknown. Here, we investigate dimers as the first intermediates in the Cu^{2+}-driven aggregation of a cyclic D,L-α-peptide architecture. The unique structural and functional properties of this model system recapitulate the self-assembling properties of amyloidogenic proteins including β-sheet conformation and cross-interaction with pathogenic amyloids. We show that a histidine-rich cyclic D,L-α-octapeptide binds Cu^{2+} with high affinity and selectivity to generate amyloid-like cross-β-sheet structures. By taking advantage of backbone amide methylation to arrest the self-assembly at the dimeric stage, we obtain structural information and characterize the degree of local order for the dimer. We found that, while catalytic amounts of Cu^{2+} promote aggregation of the peptide to fibrillar structures, higher concentrations dose-dependently reduce fibrillization and lead to formation of spherical particles, showing self-assembly to different polymorphs. For the initial self-assembly step to the dimers, we found that Cu^{2+} is coordinated on average by two histidines, similar to self-assembled peptides, indicating that a similar binding interface is perpetuated during Cu^{2+}-driven oligomerization. The dimer itself is found in heterogeneous conformations that undergo dynamic exchange, leading to the formation of different polymorphs at the initial stage of the aggregation process.

Received 26th November 2021,
Accepted 21st February 2022

DOI: 10.1039/d1cp05415e

rsc.li/pccp

Introduction

Self-assembly of proteins into oligomers and amyloid fibers lies at the heart of a variety of neurodegenerative diseases, such as Alzheimer's and Parkinson's diseases and further synucleinopathies, and also plays a major role in etiologies of amyotrophic lateral sclerosis, frontotemporal dementia and diabetes.[1–5] Recent reports collectively suggest that amyloid formation is driven by liquid–liquid phase separation,[6–8] and the early-stage oligomers rather than fibrils are considered as the pathological state of these proteins.[9–18] At the early stage of aggregation, small oligomers, such as dimers, trimers or tetramers, are present only transiently and at low concentrations as larger oligomers are rapidly formed,[14,17,19] even for simple tripeptide model systems.[20,21] Attempts to trap oligomers with sufficient concentration have led to characterization of several multimers, for some of which structural information has been obtained.[15,17,22–25] However, due to the complexity of the self-assembly process,[17] low abundance, and rapid interconversion, structural information on the small oligomers, such as dimers, is largely limited. At the same time, understanding the initial aggregation steps and the properties of these oligomers is highly sought after for a molecular understanding of the early steps towards different polymorphs that might be connected to

[a] *Department of Chemistry and Applied Biosciences, ETH Zürich, 8093 Zürich, Switzerland. E-mail: gunnar.jeschke@phys.chem.ethz.ch*
[b] *NMR-based Structural Biology, Max Planck Institute for Biophysical Chemistry, 37077 Göttingen, Germany. E-mail: cigr@mpinat.mpg.de*
[c] *Institute for Chemistry and Biology of the Marine Environment, University of Oldenburg, 26129 Oldenburg, Germany*
[d] *Department of Chemistry, Bar-Ilan University, Ramat-Gan 5290002, Israel. E-mail: rahimis@biu.ac.il*
[e] *Bar-Ilan Institute for Technology and Advanced Materials (BINA), Bar-Ilan University, Ramat-Gan 5290002, Israel*

† Electronic supplementary information (ESI) available. See DOI: 10.1039/d1cp05415e

‡ These authors contributed equally.

different pathologies[26] for example by generating varying extents of reactive oxygen species.[27–31] Also, the factors that trigger the aggregation process in cells remain elusive. A dysfunctional metal homeostasis leading to elevated concentrations of metal ions is one of the presently debated factors that may contribute to increased aggregate formation. For example, the metal-assisted self-assembly of amyloid-β protein (Aβ) or α-synuclein into soluble aggregates and amyloids has been linked to the etiologies of Alzheimer's and Parkinson's diseases.[5,27,32–38] Once the aggregation process has been started, current models suggest that cell-to-cell transmission of aggregates or oligomers rather than the formation of fibrils is responsible for the disease onset and progression.[3,13–15,18] This complexity inherent to the natural amyloidogenic systems renders the important structural characterization by biophysical methods impractical.

A far simpler system that still shares many of the amyloid properties, such as metal-binding driven self-assembly with different polymorphs, is the cyclic D,L-α-peptide architecture.[39–41] Such cyclic peptides with an even number of alternating D- and L-α-amino acids can form flat and ring-shaped conformations. Under conditions that favour hydrogen bonding and depending on their side chains and the external environment, cyclic D,L-α-peptides can stack on top of each other through a complementary intermolecular hydrogen-bonding network to form hollow and cross-β-sheet-like tubular structures (Scheme S1A, ESI†).[39,40] The cross-β-sheet conformations exhibited by cyclic D,L-α-peptides closely resemble those of pathogenic amyloids formed from Aβ, α-syn and tau-derived AcPHF6, and this similarity is most likely responsible for their cross interaction and modulation of aggregation.[30,34,41–47] For model tripeptides, non-classical cross-β-sheet structures have been found during oligomerization.[21]

In contrast to natural amyloids and natural polypeptides, the aggregation of cyclic D,L-α-peptides can be specifically arrested at the stage of dimers,[40] which allows to obtain structural information and probe the degree of local order early on in the aggregation process.

Previously, we have shown that the His-rich cyclic D,L-α-peptide **1** [HwWhHhHk] (where the upper and lower case letters represent L- and D-amino acid residues, respectively, while square brackets indicate a cyclic structure; Scheme 1) effectively self-assembles to generate amyloid-like nanostructures and induces peroxidase-like activity to protect cells from oxidative stress.[48] Such catalytic and antioxidant activities were also reported to characterize other self-assembled amyloidogenic systems, such as Aβ and α-syn.[16,28,35,49,50]

In this study, we used different complementary techniques to study the metal chelation properties of the cyclic D,L-α-peptide **1**. Similarly to Aβ whose aggregation is modulated by copper binding to histidines, the aggregation (or alternatively self-assembly) of cyclic D,L-α-peptide **1** is also affected by Cu^{2+} through interaction with His residues to generate amyloid-like nanostructures that can be reversibly controlled by Cu^{2+} or ethylenediaminetetraacetic acid (EDTA). Using backbone amide methylation to generate **3** (Scheme 1),[51] we limit the aggregation process to dimer formation.[40] This allows us to obtain structural information by spectroscopic methods such as nuclear magnetic resonance (NMR) and electron paramagnetic resonance (EPR) spectroscopies and to probe whether a well-defined dimer is generated at the first step of the self-assembly. We find that the early aggregates of cyclic peptides formed due to the metal ion coordination are highly heterogeneous dimers that are in exchange with each other. Given the observation of polymorphism of fibril structures, our results suggest that polymorphism can be detected even at the level of the dimer.

Results and discussion

Many amyloidogenic proteins bind metal ions, such as Cu^{2+}, *via* histidine residues and this interaction influences the aggregation kinetics.[5,27,32–38] Mimicking such Cu^{2+}-induced self-assembly in a minimal peptide model system, we recently developed a cyclic D,L-α-peptide octamer **1** (Scheme 1) containing multiple His residues. This system reproduces several properties of amyloids, including generation of cross-β-sheet conformation and exhibiting catalytic activity, such as peroxidase activity, which was utilized to protect L6 rat skeletal muscle cells from oxidative stress-induced toxicity under hyperglycemic conditions.[48] The design of these cyclic peptides was inspired by the self-assembly to amyloids of Aβ whose sequence contains three His residues that were proposed to be involved in chelation of metal ions, including Cu^{2+} in a process that facilitated the self-assembly of monomeric Aβ and enhanced cell toxicity.[52,53] In addition, the cyclic D,L-α-peptides also contained two hydrophobic aromatic amino acids (Trp) that promote the self-assembly of the peptides in aqueous solutions and induce sufficient hydrophobicity to ensure effective partitioning in lipid membranes.[54]

Synthesis of the cyclic D,L-α-peptide analogs and study their self-assembly process

The cyclic D,L-α-peptide **1** (Scheme 1) was synthesized on a solid support and cyclized on the resin through head-to-tail cyclization.[48] This peptide was also labeled with 4-chloro-7-nitrobenzofurazan (NBD-Cl) through the free ε-amine of Lys1 to follow its self-assembly. The *N*-methylated derivative **3** was synthesized also on the resin support according to the method developed by Chatterjee *et al.*[51] and its free ε-amino group was acetylated with sodium acetate-2-^{13}C and EDC to afford analogue **4** (Scheme 1).

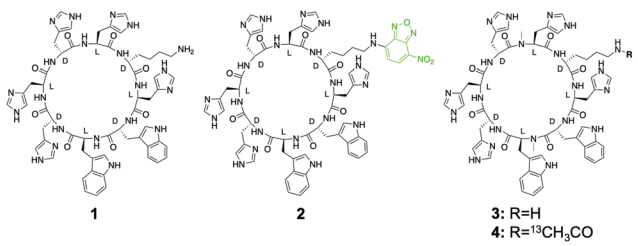

Scheme 1 Chemical structures of His-rich cyclic D,L-α-peptide analogues investigated in this study.

In order to show that **1** spontaneously self-assembles to generate amyloid-like structures, it was aged for 48 h in the presence of thioflavin T (ThT) as an indicator of amyloid formation. After a lag-phase of about 10 h, we observed a large increase in ThT fluorescence (Fig. 1A, black line), suggesting that **1** can intrinsically generate β-sheet structure, as expected.[39,41] Amyloid-like fibril formation by **1** was also confirmed by transmission electron microscopy (TEM) after 72 h of aging (Fig. 1B and Fig. S1, ESI†), which demonstrated the generation of dense and long nanotube-like bundles with 6.59 ± 0.45 nm diameter and up to 1 μm length, very similar to those reported previously.[39,48] Analysis of the high resolution TEM images revealed high crystallinity of the nanotube walls with lattice fringes of about 0.33 nm spacing that were perpendicular to the axis of the tube (Fig. S1C, ESI†). This suggests the formation of peptide nanotubes as found previously for similar cyclic D,L-α-octapeptides.[39,40]

Metal binding characterization of the cyclic D,L-α-peptide analogues

To confirm Cu^{2+} binding by the His residues present in **1**, we incubated an aqueous solution of **1** with $CuSO_4$ and then analysed it by matrix-assisted laser desorption/ionization (MALDI) mass spectrometry. Fig. 1C shows the mass analysis of an equimolar solution of **1** and $CuSO_4$. The spectrum consists of the molecular mass of the peptide (m/z = 1186.5 g mol^{-1}) and two additional peaks at 1208.5 and 1248.4 g mol^{-1} that correspond to the Na^+ and Cu^{2+} adducts of the peptide, respectively. The peak at m/z = 1248.4 g mol^{-1} does not appear in the mass spectrum of the peptide alone, showing that **1** is able to chelate Cu^{2+}.

The ability of **1** and its NBD-conjugated analogue **2** to chelate Cu^{2+} was also monitored by UV/Vis and fluorescence spectroscopy. The gradual addition of Cu^{2+} to **1** or **2** in a 1 : 1 solution of DMSO in MES buffer dose-dependently decreased both the absorbance of **1** (at 230 and 350 nm, Fig. S2A, ESI†) and the fluorescence of **2** (Fig. 1D). The decrease of NBD fluorescence is most likely due to self-quenching of the NBD moieties by Cu^{2+}-assisted self-assembly of the peptide, since similar self-quenching of NBD fluorescence has been observed in other self-assembling systems.[55] Further, reduction in the fluorescence intensity of **2** was also observed in the absence of Cu^{2+} when the total concentration of DMSO in solution was

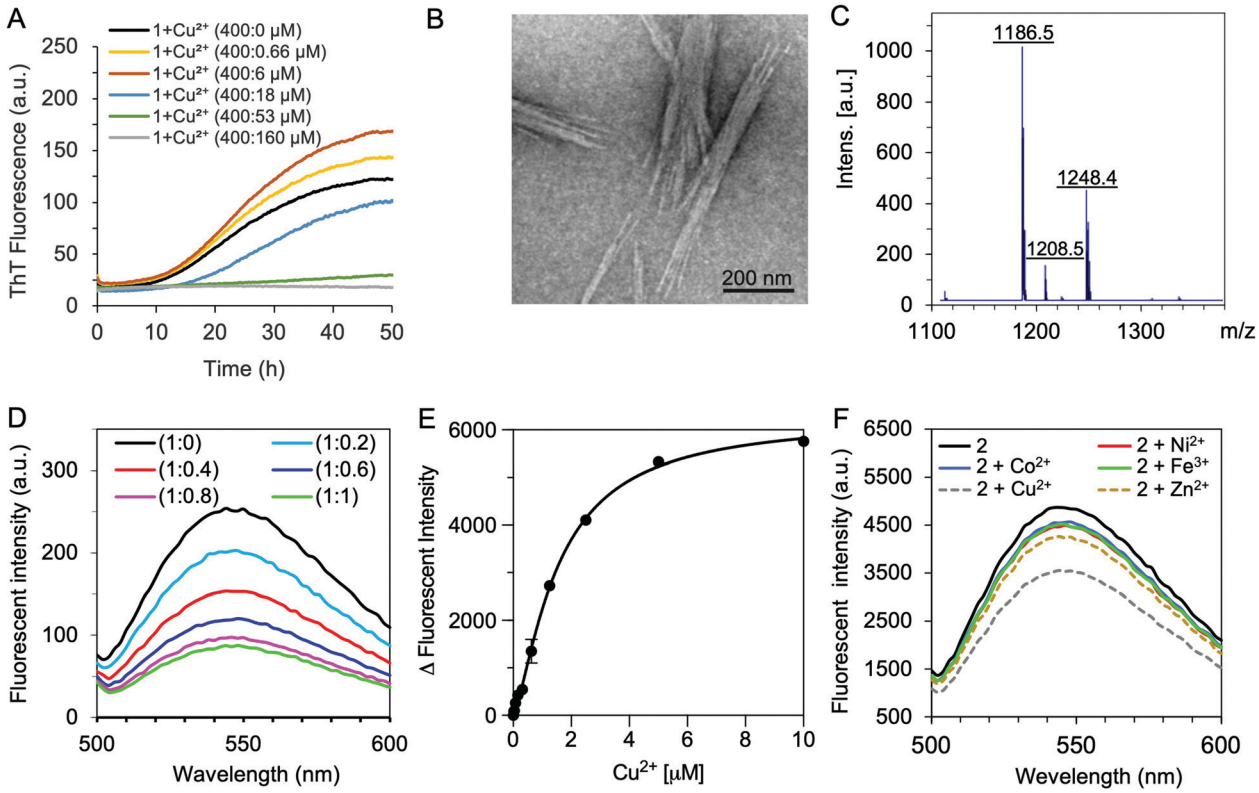

Fig. 1 Effect of Cu^{2+} on the spontaneous self-assembly of cyclic D,L-α-peptides **1** and **2**. (A) ThT fluorescence kinetics of **1** in the absence or presence of increasing amounts of Cu^{2+}. Monomeric **1** (400 μM) was incubated at 30 °C in a ThT solution (20 μM, 50% DMSO and MES (25 mM, pH 7.2)) in the absence or presence of Cu^{2+}, and the fluorescence was monitored over time. (B) Spontaneous aggregation of cyclic D,L-α-peptide **1**. TEM image of **1** (400 μM) aged for 72 h in DMSO and MES (1 : 1) solution (negatively stained sample). (C–F) Metal-chelating property of cyclic D,L-α-peptide **1**. (C) MALDI-TOF mass spectrum of **1** (0.22 mM, calc. m/z (**1**–H^+) = 1186.3 g mol^{-1}) with an equimolar mixture of $CuSO_4$ (calc. m/z (**1**–H^+ + Cu^{2+}) = 1248.8 g mol^{-1}). (D) Fluorescence spectra ($\lambda_{ex.}$ = 470 nm) of **2** (1 μM) in a DMSO and MES (1 : 1) solution in the presence of increasing amounts of Cu^{2+}, expressed as the molar ratio of **2** : Cu^{2+}. (E) Fluorescence titration of **2** (1 μM) in the presence of increasing amounts of Cu^{2+} showing a saturable binding curve. Absolute values are shown. (F) Cyclic D,L-α-peptide **2** binds selectively to Cu^{2+}. Cyclic peptide **2** (1 μM) was incubated with various metals (1 μM) and the fluorescence signal was measured after 60 min. Data in (A and D–F) are representative of three-independent experiments that yielded similar results.

gradually decreased (Fig. S2B, ESI†) or the solution was incubated for a prolonged time (Fig. S2C, ESI†), confirming the spontaneous self-assembly of the cyclic D,L-α-peptides as shown also by the ThT fluorescence assay (Fig. 1A). The spontaneous self-assembly of **1** is most likely mediated by intermolecular aromatic interactions between Trp residues and hydrogen bonds generated between the cyclic D,L-α-peptides.[39,40]

The UV/Vis titration studies of **1** with $CuSO_4$ were consistent with the formation of a peptide : Cu^{2+} complex with an average stoichiometry of 1 : 2.5 (Fig. S2D, ESI†). Further, fluorescence titration of **2** with increasing concentrations of $CuSO_4$ as a ligand showed a saturable binding curve with apparent dissociation constant (K_d) of 1.5 μM for formation of the Cu^{2+}–**2** complex (Fig. 1E). The fluorescence intensity of **2** was also followed for Zn^{2+}, Fe^{3+}, Co^{2+}, and Ni^{2+} to determine whether chelation is metal specific. The cupric ion was found to bind best to **2**, followed by Zn^{2+}, as may be expected from a His-rich polypeptide. Other metal ions influenced the fluorescence of **2** only slightly, suggesting the selectivity of the cyclic peptides for Cu and Zn ions (Fig. 1F).

The affinity and selectivity of **2** toward different metals were confirmed by the MicroScale Thermophoresis (MST). MST has been widely applied to determine the interaction between macromolecules or even cell components with small molecules or ions.[56–58] The binding affinity obtained with MST for Cu^{2+} and **2** was very similar to those obtained from the fluorescence intensity and therefore it was used to determine and compare the K_d values of other metals. Collectively, the MST results confirm those obtained from the fluorescence studies and suggest that **2** binds with similar affinity Cu^{2+} (K_d = 1.78 ± 0.16 μM) and Zn^{+2} (K_d = 2.82 ± 0.20 μM), while it has a significantly lower affinity for Ni^{2+} (K_d = 13 ± 1.14 μM), Fe^{3+} (K_d = 150 ± 34.5 μM) and Co^{2+} (K_d = 287 ± 20.4 μM).

Effect of Cu^{2+} on self-assembly and aggregation of the cyclic D,L-α-peptides 1 and 2

Since copper showed the highest binding affinity to the peptide, we tested its effect on the self-assembly of **1**. In ThT fluorescence experiments, we found that the presence of catalytic amounts of Cu^{2+} (1 : 0.0016 and 1 : 0.015, **1** : Cu^{2+}) significantly increased the ThT fluorescence, while higher concentrations of Cu^{2+} (>1 : 0.045) significantly decreased the ThT fluorescence and prolonged the kinetic lag phase (Fig. 1A). These results suggest that catalytic concentrations of Cu^{2+} enhance the self-assembly and aggregation of **1**, while higher, but still substoichiometric concentrations of Cu^{2+} either inhibit the formation of the fibrils or led to the generation of aggregates that do not bind ThT. Alternatively, the reduction in ThT fluorescence might be attributed to the quenching effect of the free paramagnetic Cu^{2+} (see below). A similar effect of Cu^{2+} on aggregation kinetics and a possible quenching effect of the ThT fluorescence were reported when Aβ was incubated with increasing concentrations of Cu^{2+}.[30,45,47,59]

Further evidence for the metal-induced self-assembly of **1** was provided by TEM and atomic force microscopy (AFM). Samples were collected from the kinetic ThT assays performed

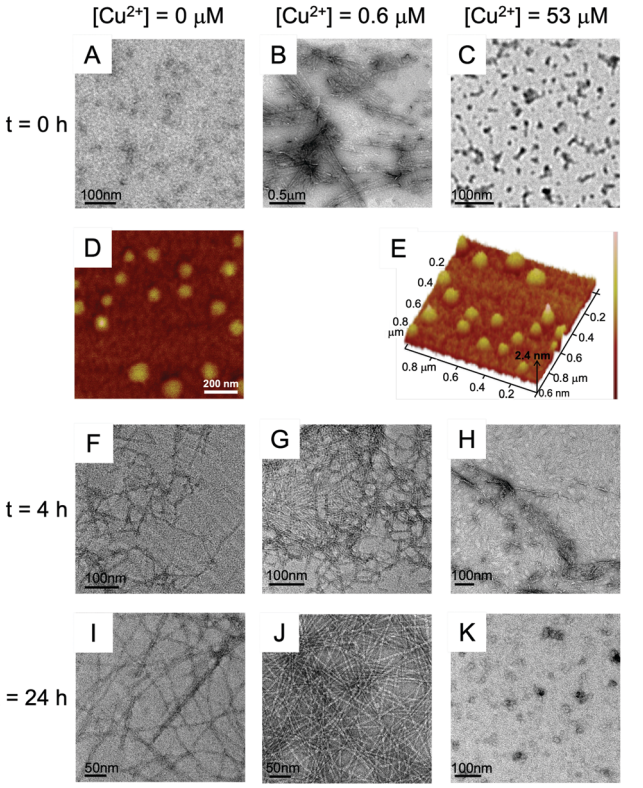

Fig. 2 Effect of Cu^{2+} on the self-assembly of **1** and its morphology. TEM (A–C and F–K) and AFM (D and E) images of **1** (400 μM) incubated with increasing concentration of Cu^{2+} for 0, 4 and 24 h in DMSO : MES (1 : 1). Negatively stained samples are shown for TEM analysis.

in the absence and presence of different concentrations of Cu^{2+} and analysed by TEM and AFM. While very few peptide nanostructures with spherical structure (diameter of 30.4 ± 4.1 nm) were observed in the absence of Cu^{2+} at time t = 0 (Fig. 2A), few fibrillar structures were evident in fresh preparation of the cyclic peptide even in the presence of substoichiometric amounts of Cu^{2+} (0.6 μM; Fig. 2B). The spherical nature of the particles at t = 0 was also confirmed by AFM, which demonstrated particles with a diameter of (86 ± 18) nm (Fig. 2D and E). Interestingly, fresh solution of **1** mixed with a higher concentration of Cu^{2+} (53 μM) did not form any fibrils, but rather generated particles with a diameter of (13.2 ± 2.3) nm (Fig. 2C). Upon incubation of the mixtures for 4 h, the number of the fibrils increased in all samples prepared in the absence or presence of Cu^{2+} (Fig. 2F–H). However, round-shaped structures with a diameter of (45 ± 11) nm were still detectable in the samples prepared in the absence of the Cu^{2+} (Fig. S3, ESI†), and the amount of the fibrils generated in the presence of low Cu^{2+} concentration was significantly higher than the fibrils generated in the absence of Cu^{2+} or at higher concentration of Cu^{2+} (Fig. 2F–H). Mature and long fibrillar structures were observed when **1** was aged for 24 h in the absence or presence of Cu^{2+} (0.6 μM; Fig. 2I and J), however the amount of the fibrils in samples incubated with low concentration of Cu^{2+} was significantly higher than that generated in the absence of Cu^{2+}, which correlates with the higher ThT

fluorescence of the sample (Fig. 1A). In sharp contrast, higher concentration of Cu^{2+} (53 μM) largely abolished the formation of the fibrils after 24 h incubation and stabilized the formation of round-shaped particles (Fig. 2K), which is again in agreement with the low ThT fluorescence of the samples. Spherical structures were also reported when Aβ was incubated with Cu^{2+}.[45] These results show that the decreased ThT fluorescence of the samples incubated with Cu^{2+} concentrations of 18 μM and higher (Fig. 1A) is directly related to the lower amount of fibrils generated rather than to a quenching effect of the ThT fluorescence by excess Cu^{2+}. Cu^{2+}-Induced nanotubular structures could be detected by TEM even in the absence of uranyl acetate used for negative staining, most probably because of the chelated Cu^{2+}. Indeed, the presence of Cu^{2+} on the fibrils was confirmed by energy-dispersive X-ray spectroscopy (data not shown).

The inhibitory effect of high concentrations of Cu^{2+} on the self-assembly and aggregation of **1** was further confirmed with dynamic light scattering (DLS). While incubation of **1** (400 μM) for 24 h generated particles with a mean size of about 0.65 μm, the presence of Cu^{2+} (800 μM) led to the formation of significantly smaller particles with a largest size intensity of about 220 nm (Fig. S4, ESI†), confirming the ThT and TEM observations. Interestingly, the DLS measurements also show a minor fraction of particles with sizes of (54 ± 12) nm, which are most likely correlated with the spherical particles also detected by TEM (Fig. 2K and Fig. S3, ESI†).

The thermodynamic properties of Cu^{2+} binding and induced self-assembly of **1** were also studied by isothermal titration calorimetry (ITC). Fig. S5 (ESI†) shows the ITC data observed upon injecting Cu^{2+} into a solution of **1** at 30 °C and corresponding fits using a model with two independent binding sites. The fitted data estimated the average stoichiometry of the binding of **1** and Cu^{2+} to be 1 : 2.3, which is in good agreement with the result obtained from the fluorescence titration. The association constant for the first binding event was determined to be about $(1.2 \times 10^7 \pm 3.9 \times 10^6)$ M^{-1} ($K_d = 8.3 \times 10^{-8}$ M), which corresponds to a standard Gibbs free energy change (ΔG°) of −9.8 kcal mol^{-1}. This reflects a favorable enthalpic contribution ($\Delta H^\circ = -15.4 \pm 0.3$ kcal mol^{-1}) and an unfavorable entropic contribution ($-T\Delta S^\circ = 5.6 \pm 1.8$ kcal mol^{-1}), which might originate from loss of conformational degrees of freedom in **1** due to the metal chelation. These values are in good agreement with the ITC values obtained for the interaction of other His-rich peptides with Cu^{2+}.[60] The second binding step is assumed to be related to the Cu-induced self-assembly process of the cyclic D,L-α-peptide with an association constant of $(6.2 \times 10^5 \pm 1.7 \times 10^5)$ M^{-1} ($K_d = 1.6 \times 10^{-6}$ M), which corresponds to a ΔG° of −8.03 kcal mol^{-1}. Most of the free energy in this reaction originates from favorable entropic contributions ($-T\Delta S^\circ = -12.75 \pm 2.1$ kcal mol^{-1}), which compensate for the unfavourable endothermic enthalpy of association ($\Delta H^\circ = 4.7 \pm 0.3$ kcal mol^{-1}). A very similar binding constant (5.3×10^5) M^{-1} was reported for the self-assembly of a 6-residue α,γ-cyclic peptide.[61] The second association constant observed by ITC of **1** in the presence of Cu^{2+} is close to those resulting from fluorescence and MST studies of the cyclic peptide **2**, where only a single binding constant was observed during the Cu^{2+}-induced self-assembly process, suggesting that in this case an effective binding constant for the Cu^{2+}-induced self-assembly is observed.

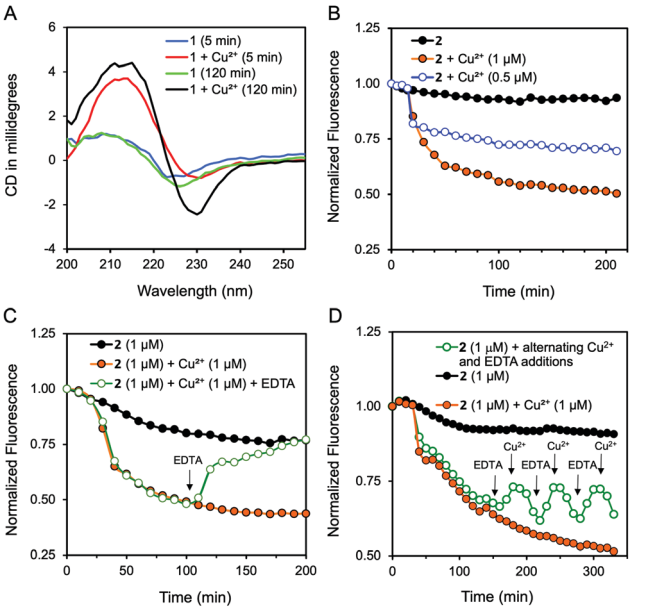

Fig. 3 Effect of Cu^{2+} on the conformation and rate of the self-assembly of **1**. (A) Time-dependent far-UV CD spectra of freshly prepared **1** (10 μM) incubated in the absence or presence of Cu^{2+} (10 μM) in MES buffer (10 mM, pH 6.6) and analyzed over time. (B) Effect of Cu^{2+} on the aggregation rate of **2**. Cyclic D,L-α-peptide **2** (1 μM) was incubated in the absence or presence of Cu^{2+} (0.5 and 1 μM) and the rate of self-assembly was monitored by following the fluorescence signal. The Cu^{2+} solution was injected into the solution of **2** after 15 min of incubation. (C) Cyclic D,L-α-peptide **2** binds Cu^{2+} reversibly. Cyclic D,L-α-peptide **2** (1 μM) was incubated in the presence of Cu^{2+} (1 μM) for 100 min to induce self-assembly. EDTA (1 μM) was then injected at once to the solution and the fluorescence signal was monitored for an additional 100 min. (D) Following incubation of **2** with Cu^{2+} for 100 min, EDTA and Cu^{2+} were added alternately and repeatedly in 20 min intervals, while monitoring the fluorescence signal. Data in (B–D) are normalized to the fluorescence of **2**.

Using circular dichroism (CD) we studied the effect of Cu^{2+} coordination on the secondary structure of **1**. In the absence of Cu^{2+}, the CD spectrum of **1** displayed a positive CD peak at around 209 nm and a negative peak at around 226 nm (Fig. 3A), which resembles the CD spectrum obtained from other cyclic D,L-α-peptides generating β-sheet structures.[41,43,44] The CD spectrum was stable even after 24 h (data not shown). Co-incubation of **1** with Cu^{2+} (1 : 1) caused an immediate increase in the CD intensity and a shift of the spectrum to positive and negative peaks at 213 and 231 nm, respectively. The negative band at 231 nm is suggestive of Trp–Trp interactions,[62,63] which are generated by Cu^{2+}-triggered self-assembly of **1** into peptide nanostructures, and therefore its intensity is enhanced over time following the addition of Cu^{2+} (Fig. 3A, black line).

The effect of metal chelation on the rate of self-assembly was confirmed by fluorescence studies. Cyclic D,L-α-peptide **2** (1 μM) was incubated with Cu^{2+} (0.5 and 1 μM) and its fluorescence was monitored over time and compared with that of **2** alone.

While the fluorescence of **2** slowly decreased over time in the absence of Cu^{2+} as a result of the spontaneous self-assembly of the cyclic D,L-α-peptide scaffold, the addition of Cu^{2+} dramatically enhanced the self-assembly rate, as revealed by the fast reduction in the fluorescence signal (Fig. 3B). These results also suggest that the direct fluorescence measurement of **2** to determine its rate of self-assembly and aggregation is more sensitive to early self-assembly steps than ThT-based experiments because kinetics by fluorescence quenching could be detected during the lag phase of about 10 h of the ThT assay (Fig. 1A) during which dimers or other small oligomers are formed, while changes in ThT-based fluorescence require formation of more mature fibrillar structures.

Having shown that the binding of Cu^{2+} to **1** promotes the self-assembly of the latter, we next determined whether this process is reversible. Peptide **2** (1 μM) was incubated with Cu^{2+} (1 μM) for 100 min to induce self-assembly, which was followed by a reduction in fluorescence intensity (Fig. 3C, green line). EDTA was added in excess and the fluorescence was monitored further for 100 min. An increase in the fluorescence intensity back to the level of **2** in the absence of Cu^{2+} was observed, most probably due to disassembling the preformed metal-induced aggregates to monomeric peptide. Similar results were reported for the metal-mediated assembly of Aβ[41] and collagen-based peptides.[64–66] Notably, we found that the aggregation and disaggregation processes of **2** are fully reversible over repeated cycles of Cu^{2+} and EDTA additions (Fig. 3D), resembling the activity of molecular switches that can perform simple "ON" and "OFF" operations.[67]

Study the effect of Cu^{2+} on the structure of cyclic D,L-α-peptide analogues

In order to obtain structural information on the interaction of **1** and Cu^{2+} and the Cu^{2+}-induced self-assembly, electron paramagnetic resonance (EPR) and nuclear magnetic resonance (NMR) spectroscopies were used. These methods also helped to decipher how His-nitrogens coordinate Cu^{2+}.

EPR studies

The cw EPR spectrum of paramagnetic Cu^{2+} has a strong *g*-anisotropy and a four-fold hyperfine splitting due to its nuclear spin $I = 3/2$. The spin Hamiltonian parameters, the *g*- and A-tensors describing the Zeeman and the hyperfine interaction, respectively, are known to be correlated to the type of atoms present in the first coordination shell of Cu^{2+}, for which Cu^{2+} favours square planar coordination.[68]

In cw EPR titration experiments, incubation of **1** (0.4 mM) with increasing concentrations of Cu^{2+} for 0 and 24 h generated an overall broad spectral shape most likely due to variability in the Cu^{2+} coordination geometries (Fig. 4A). The similar $A_{\parallel}$ hyperfine splitting, resolved on the low-field side of the spectra and observed up to 2 mM of Cu^{2+}, suggests that the first-shell coordination environment of peptide-bound Cu^{2+} does not change for concentrations between 133 μM and 2 mM. This spectral component becomes saturated (Fig. 4B) at a Cu^{2+} concentration of 0.8 mM and higher, corresponding roughly to a ratio of one Cu^{2+} per two histidine residues of **1**. At Cu^{2+} concentrations of 2 mM and higher, a combination of **1**-bound Cu^{2+} and free $[Cu(H_2O)_6]^{2+}$ becomes visible in the spectra. These results are in good agreement with those obtained from a Job's plot using UV/Vis spectroscopy (Fig. S2D, ESI†). The EPR signal of low concentrations of free Cu^{2+} appears to be

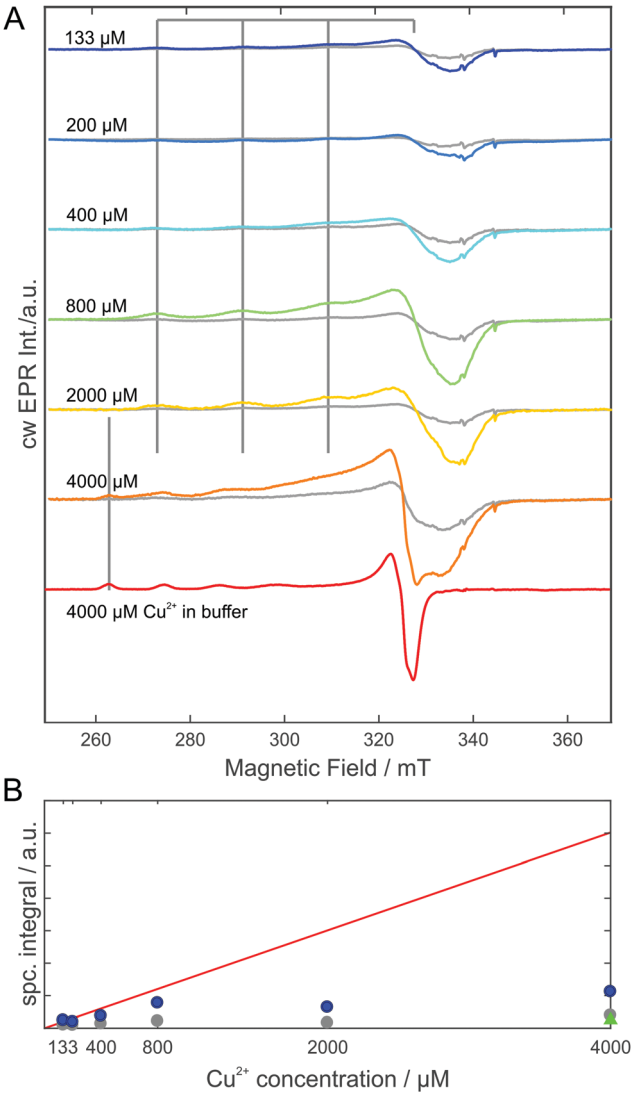

Fig. 4 Cu^{2+}-Titration series of **1** showing increasing uptake over time. (A) Cw EPR spectra at 20 K of 400 μM **1** incubated with increasing amounts of Cu^{2+} (as indicated) for 0 (grey) and 24 hours (coloured). Signal intensity increase shows Cu^{2+} uptake over time. The similarity of the spectral lineshapes, seen by equal Cu^{2+} hyperfine splittings (set of four vertical grey lines), suggests a Cu^{2+} coordination largely independent of its concentration (*cf.* Fig. S6 and S7, ESI†). At high copper concentrations the spectral component of free Cu^{2+} becomes visible (single grey line indicates a non-overlapping peak in the control without **1**). (B) Relative EPR-visible Cu^{2+} concentration is quantified by double integration of the cw EPR spectra and compared to Cu^{2+} + 100 mM imidazole (red line). Free Cu^{2+} in buffer remains largely EPR silent, even at a concentration of 4 mM (green triangle). After 24 h incubation time with **1** (400 μM) (blue circles), the fraction of Cu^{2+} detected by EPR increases for all Cu^{2+} concentrations as compared to 0 h incubation time (grey circles), reflecting its coordination by the cyclic peptide and an uptake of Cu^{2+} onto the peptide assembly.

suppressed by the MES buffer as has been described for NEM buffer.[69] Upon an incubation time of 24 h, we observed a significant increase of the EPR signal intensity without a change in the spectral shape, indicating an increase in the fraction of EPR-visible Cu^{2+} (Fig. 4 and Fig. S6A, ESI†). Fig. 4 also shows the $g_{\parallel}$ region of the spectra and the Cu^{2+} $A_{\parallel}$ hyperfine quartet in the field range from about 260 to 320 mT, from which we determined the corresponding $g_{\parallel}$ and $A_{\parallel}$ values. These parameters have been used by Peisach and Blumberg to investigate the coordination of type 2 Cu^{2+} sites.[68] We have compared our experimental results to the empirically known Peisach–Blumberg correlations for $g_{\parallel}$ and $A_{\parallel}$ values, which gives insight into the first, square-planar Cu^{2+}-coordination shell (Fig. S6B, ESI†). The results are consistent with several Cu^{2+} coordination modes. Taking into account that the net charge of the coordination site is not likely to be strongly negative for the peptide, the analysis indicates that on average at least two nitrogen atoms are directly coordinating Cu^{2+}.

We further used the pulsed EPR techniques ESEEM[70] and its 2D variant HYSCORE[71] to detect weakly coupled nuclei, such as non-coordinating nitrogens (^{14}N, I = 1), in the vicinity of paramagnetic Cu^{2+}.[72–74] Histidine, which is abundant in **1**, coordinates Cu^{2+} directly *via* one nitrogen atom leading to a strong hyperfine coupling for that nitrogen. This leaves the second nitrogen atom in the regime of weak hyperfine coupling. Probing for such weakly coupled nitrogens around Cu^{2+}, 3-pulse-ESEEM (3pESEEM) data obtained from **1** (400 μM) in the presence of increasing concentrations of Cu^{2+} up to 2 mM shows pronounced oscillations that stem from nitrogens and protons, while in case of Cu^{2+} (4 mM) modulation from solvent protons dominates (Fig. S7, ESI†). This is in agreement with the water-coordinated Cu^{2+} observed in the cw EPR experiments at this concentration. Moreover, similar to the cw EPR results, the local Cu^{2+} environment appears to be unchanged in the Cu^{2+} concentration range from 200 to 800 μM. As better spectra can be obtained at higher concentrations, more detailed studies were focused on the system with 400 μM **1** and 800 μM Cu^{2+}.

The 3pESEEM data of **1**, recorded at a proton blind spot to enhance nitrogen sensitivity, and the corresponding cross-term averaged[75] and Fourier transformed spectra (Fig. 5A and B) are dominated by the nitrogen quadrupolar interaction with three principal transitions below 2 MHz and a broader double-quantum transition around 4 MHz.[76,77] The *N*-methylated analogue of **1**, the cyclic D,L-α-peptide **3** (Scheme 1) forms only dimers, as the methyl groups block further stacking.

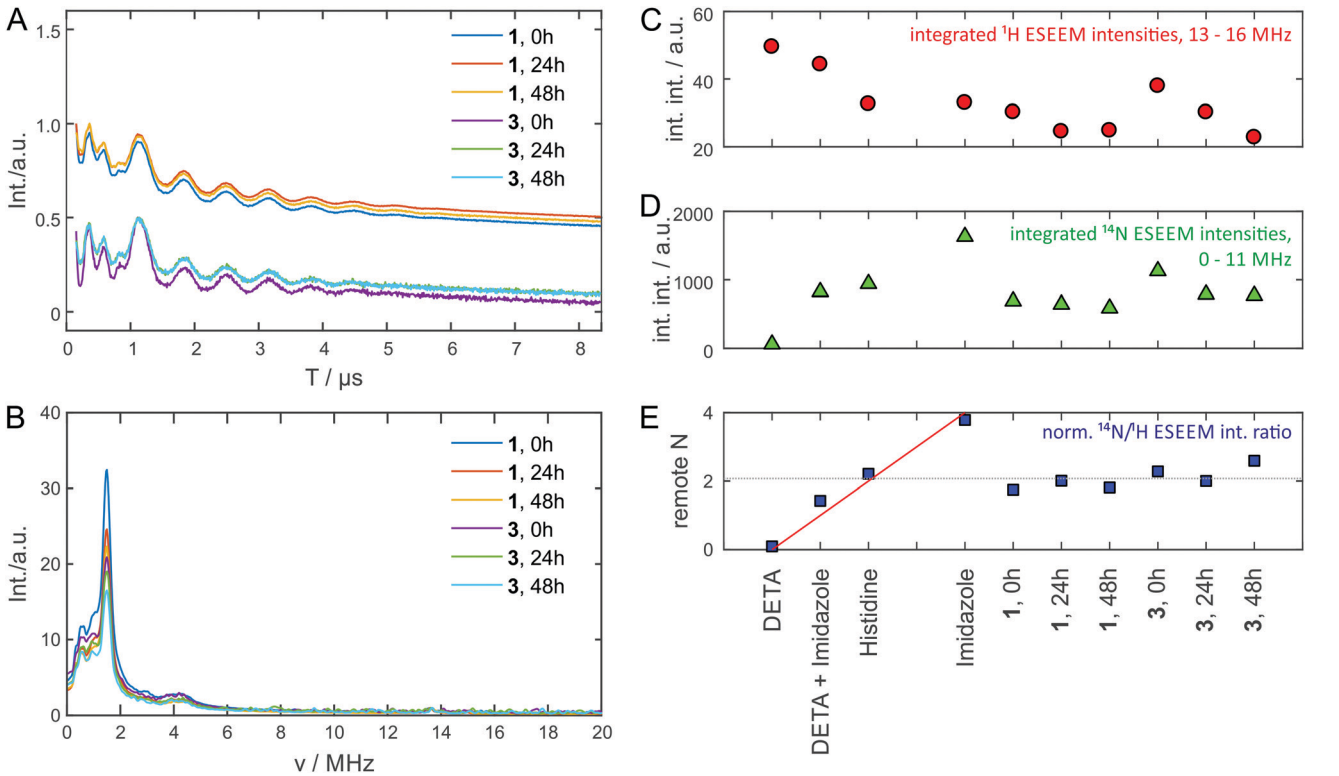

Fig. 5 Analysis of weakly coupled nitrogens by 3-pulse-ESEEM. (A) The intensity-normalized 3pESEEM time traces of **1** and the *N*-methylated analogue **3** (offset for clarity after normalization), and (B) the Fourier transform (FT) spectra (analysed with cross-term averaging) normalized to the proton intensity showing the coupling of weakly coupled nitrogens. To quantify the number of nitrogens, FT spectra (as in (B), without cross-term averaging, see Fig. S8D, ESI†) were integrated over (C) the proton frequencies and (D) the weakly coupled nitrogen frequencies. (E) The ratio of the integrated intensities in C and D is proportional to the number of the weakly coupled nitrogens, as validated using the four model compounds with zero (diethylenetriamine (DETA)) to four (imidazole) weakly coupled nitrogens (see Fig. S8, ESI†). The ratio is fitted by linear regression (red) and subsequently normalized to the number of weakly coupled nitrogens. The average value for all the peptide/Cu^{2+} samples (grey line) indicates an average number of ~2 weakly coupled nitrogens.

The ESEEM spectra of **1** and **3** in the presence of Cu^{2+} are very similar, suggesting that the observed Cu^{2+} coordination environment can be understood in terms of the dimer structure. By comparing the spectra obtained from mixtures of **1** and Cu^{2+} to those of model compounds featuring different numbers of weakly coupled nitrogens, namely 0, 1, 2 or 4 (Fig. S8, ESI†),[72,78,79] we found that the spectra of **1** closely resemble that with two weakly coupled nitrogens of bis-histidine-coordinated Cu^{2+}. A similar approach was applied to study the local coordination of Cu^{2+}-bis-histidine in a fibrillary Aβ peptide fragment.[77] In contrast to the previous study,[77] we observe broader ESEEM spectra for **1** and **3** that indicate some local variation in the Cu^{2+} coordination geometry.

We quantified the number of weakly coupled nitrogens around a Cu^{2+} ion by integrating the nitrogen region in the 3pESEEM spectra, using the proton signal as a ref. 72. A similar analysis was also used in earlier studies to quantify the number of deuterium atoms around a nitroxide spin label.[80] Accordingly, the 3pESEEM spectra evaluated without cross-term averaging of **1**, **3** and the model compounds (Fig. S8, ESI†) incubated in the of presence Cu^{2+} were integrated over the ^{14}N-spectral range and normalized by the integral over the proton range (Fig. 5C–E). The resulting $^{14}N/^{1}H$ intensity ratio (Fig. 5E) shows a linear dependence on the number of weakly coupled nitrogens for the model compounds, as expected from literature.[72] In the spectra obtained from incubation of the cyclic D,L-α-peptides **1** with Cu^{2+}, this intensity ratio appears constant for all incubation times. Linear regression yields an average number of 1.9 ± 0.2 weakly coupled nitrogens in the Cu^{2+} coordination environment. A similar value of 2.3 ± 0.3 is also found for the dimeric Cu^{2+} complex of **3**. Therefore, the majority of the Cu^{2+} sites in both cases feature two weakly coupled nitrogens, which may either reside in the imidazole rings of Cu^{2+}-coordinating histidine residues or in the peptide backbone. This conclusion is further corroborated by HYSCORE spectra of **1**-Cu^{2+} complex as well as the model compounds shown in Fig. 6 and Fig. S9, S10 (ESI†). Like the 3pESEEM spectra obtained from **1** and Cu^{2+} with different incubation times (0, 24 and 48 h) (Fig. 5), the corresponding HYSCORE spectra are largely similar and show an intensity pattern similar to the bis-histidine-Cu^{2+} model

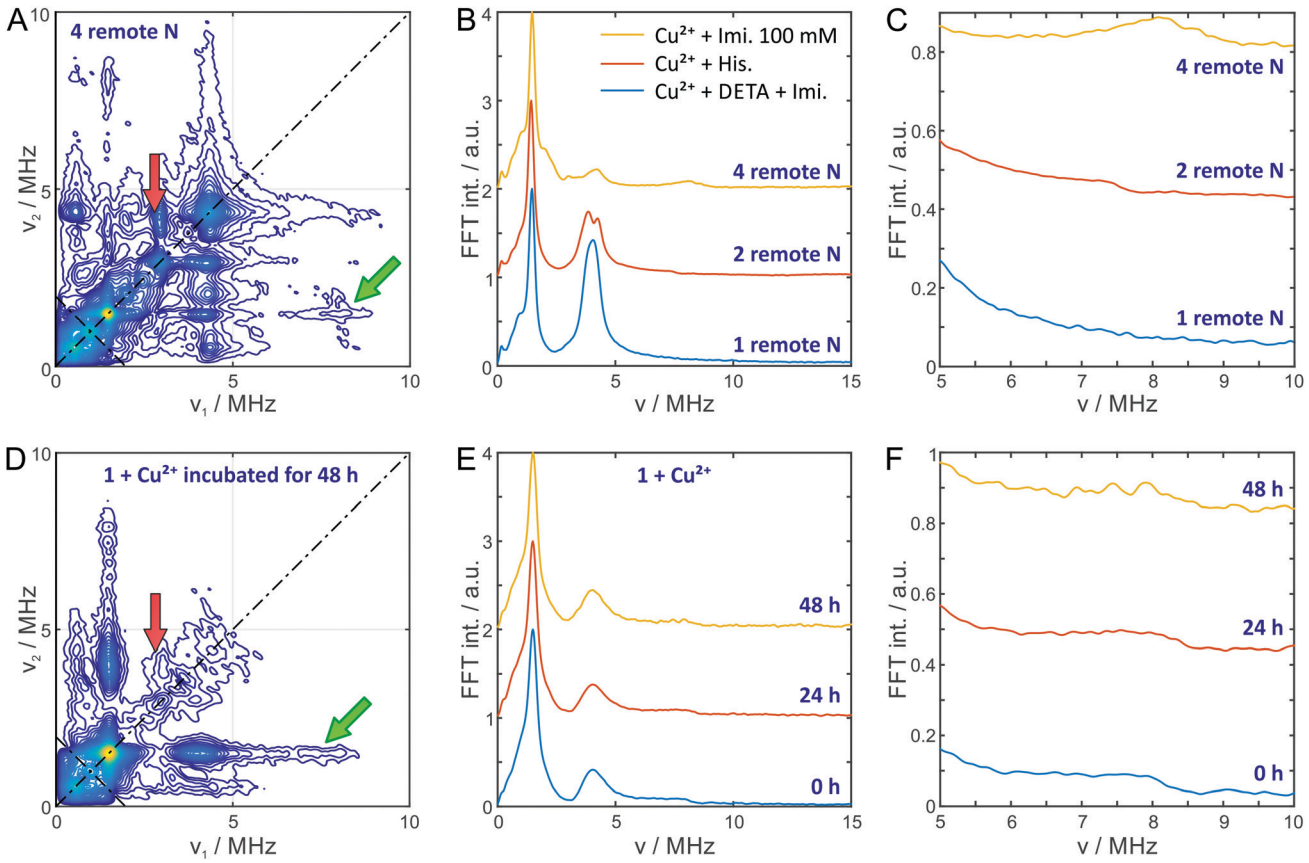

Fig. 6 Assessing the presence of hyperfine couplings to two weakly coupled (remote) ^{14}N by HYSCORE. (A) HYSCORE spectrum of imidazole-coordinated Cu^{2+} featuring four weakly coupled ^{14}N, where cross peaks in the double quantum region (red arrow) and a weak two-nitrogen double quantum transition (green arrow) are observed. (B) 1D slices from the 2D spectra (in (A) and Fig. S9, ESI†) are averaged over both dimensions for 1.35–1.65 MHz showing the relative intensities of the 2 × ^{14}N-double-quantum transitions for the Cu^{2+}–^{14}N model compounds. (C) Zooming into the region shows a clear absence of transitions around 8 MHz in case of a single weakly coupled ^{14}N and increasingly visible spectral intensity for two and four weakly coupled ^{14}N. Analogous HYSCORE data for **1** (400 μM) incubated with Cu^{2+} (800 μM) for different times is shown in (D–F) and Fig. S10 (ESI†). (F) The two-nitrogen double-quantum transitions observed for all three peptide samples indicate the presence of Cu^{2+} coordinated by at least two weakly coupled ^{14}N.

compound (Fig. 6). Particularly, two features in the spectra underline this similarity. First, the intensity ratios of ^{14}N single and double-quantum transitions of the **1** + Cu^{2+} spectrum strongly resemble those of bis-histidine-Cu^{2+} (Fig. S9 and S10, ESI†); and second, the two-nitrogen double-quantum transition around 8 MHz (green arrow in Fig. 6) is discernible from the noise level in the 1D projections (Fig. 6C and F), which is an unambiguous indicator of species with two or more weakly coupled nitrogens.[77] This feature is visible in the spectra of **1** + Cu^{2+} as well as in the model compound spectra with two and four weakly coupled nitrogens with an intrinsically low intensity due to the low probability of this transition. Therefore, in agreement with the 3pESEEM spectra (Fig. 5 and Fig. S8, ESI†), the HYSCORE spectra point towards two nitrogens that are weakly coupled to Cu^{2+} from coordination by two histidine residues. An alternative assignment to backbone nitrogens, when the adjacent carbonyl oxygen directly coordinates Cu^{2+},[81,82] appears unlikely considering that backbone oxygens are also involved in inter-peptide hydrogen bonding. Furthermore, the HYSCORE spectrum of **3** + Cu^{2+} shows the same nitrogen couplings in spite of the partial backbone *N*-methylation, which suggests a similar Cu^{2+} coordination for dimer and fibrils.

The coordination of Cu^{2+} to **1** was further probed by the pulse EPR techniques ELDOR-detected NMR (EDNMR) and the recently developed CHEESY-detected NMR that allow to analyse moderately-sized hyperfine couplings with high sensitivity.[83] The spectra shown in Fig. S11 and S12 (ESI†) reveal both strongly and weakly coupled nitrogens for the model compounds as well as for **1**. The stronger couplings, which correspond to nitrogens directly coordinated to Cu^{2+}, vary significantly for the different model compounds. For the cyclic peptide **1**, they appear broadly distributed so that individual couplings cannot be distinguished, similar to what we observe for the weakly coupled nitrogens. Hence, the ELDOR-detected NMR spectra support the notion of Cu^{2+} coordination by histidine with a broad distribution of local coordination geometries even if the number and type of coordinating atoms may not vary. The experimentally observed Cu^{2+} coordination by on average two histidines is consistent with the sterically permissive coordination geometries on a peptide nanotube, which span one to three histidine residues (Fig. S13, ESI†).

Since the Cu^{2+}-induced self-assembly of **1** should lead to close proximity of Cu^{2+} ions, we probed for the presence of Cu–Cu distances by the EPR technique Double Electron–Electron Resonance (DEER).[84,85] We assumed that the self-assembly of Cu-bound **1** to amyloid-like structures, would cause the juxtaposition of Cu atoms, in which case their inter-spin distance could be measured by DEER. Using this technique, Cu^{2+}–Cu^{2+} distances have been resolved in many systems, where two Cu^{2+} ions were bound at distinct sites.[86–88] Fig. S14 (ESI†) shows the putative proximity of Cu atoms along the assembled **1** or **3**, using 4-pulse DEER. The results show a fast decay of the dipolar modulation indicating inter-spin distances shorter than 1.5 nm and hence below the quantification limit by DEER, along with a slower background decay. Both the fast and slow decay components are slightly faster for **1** compared to **3**, indicating a higher local Cu^{2+} concentration for the self-assembled **1**. This is in agreement with significantly faster spin–lattice relaxation times measured for **1** (Fig. S15, ESI†) as compared to those measured for the model compounds and for the *N*-methylated peptide **3** that can self-assemble only to dimers. The number of interacting spins given by the DEER modulation depth remains approximately equal for 0, 24, and 48 h incubation time, indicating that DEER is not sensitive to fibril formation. This in turn suggests that the Cu^{2+} ions involved in this process reside at binding sites with minimal distances shorter than 1.5 nm, below the interpretable distance range of DEER. Notably, the intermolecular distance between equivalent sites in two adjacent cyclic peptides in the assembly is estimated to be 0.47 nm.[39] In summary, the EPR data collectively suggest that Cu^{2+} binds **1** through coordination of at least two histidine residues and that the dimer features a distribution of copper coordination geometries, which is also present in the fibrils.

NMR studies

It has been reported by Ghadiri and co-workers that the backbone of the cyclic peptides with even number of alternating D- and L-amino acids adopts a low-energy flat ring-shaped conformation with N–H and C═O groups pointing perpendicular to the plane of the ring. The observed large $^3J_{NH-H\alpha}$ couplings (6.4–8.4 Hz) in the ^{1}H NMR spectra and strong $NH_{(i)}/H\alpha_{(i+1)}$ NOE correlations are in good agreement with the flat ring-shaped conformation of the backbone of the cyclic peptides **1** and **3** (Fig. S16 and Tables S1, S2, ESI†). The ability of Cu^{2+} chelation of **1** and **3** was monitored by recording ^{1}H NMR titration spectra with increasing amounts of Cu^{2+}. Cu^{2+} concentration dependent attenuation of histidine imidazole side chain $H_{\varepsilon1}$ and $H_{\delta2}$ protons (Fig. 7) suggests that all 5 histidines including the isolated His-8 of **1** and **3** are involved in Cu^{2+} coordination, which agrees with the UV-Vis and EPR spectroscopy derived stoichiometry of 1 : 2.5 peptide : Cu^{2+}, in agreement with dimer formation with a molar ratio of 2 : 5 peptide : Cu^{2+}. Therefore, a similar Cu^{2+} coordination environment is expected for both **1** and **3**. However, at 0.4 molar equivalents of Cu^{2+}, all the proton resonances vanished in the spectrum, which hinders the study of fully saturated complex of **1** or **3** with Cu^{2+} (Fig. 7). The aggregation of **1** was monitored by acquiring a series of ^{1}H NMR spectra of 800 μM of **1** in 1 : 1 DMSO-D_6/MES (25 mM, pH 7.2) at 303 K. The consumption of peptide monomer over a period of 24 h indicates the spontaneous aggregation of **1** (Fig. S17, ESI†). Presence of substoichiometric equivalents of Cu^{2+} enhanced the aggregation of **1** (Fig. S17D, ESI†), which is in agreement with the observations from ThT fluorescence and TEM analysis. No new signals appeared and no line broadening of proton resonances was observed in the ^{1}H NMR spectra of **1**, suggesting that the oligomers and fibrils formed are not observable in the NMR spectrum and the signal decay is purely due to the depletion of the cyclic peptide monomer. In order to better understand the Cu^{2+} concentration dependent morphological changes of cyclic peptide self-assembly, one needs to characterize the early oligomeric species, which act as a seed for further

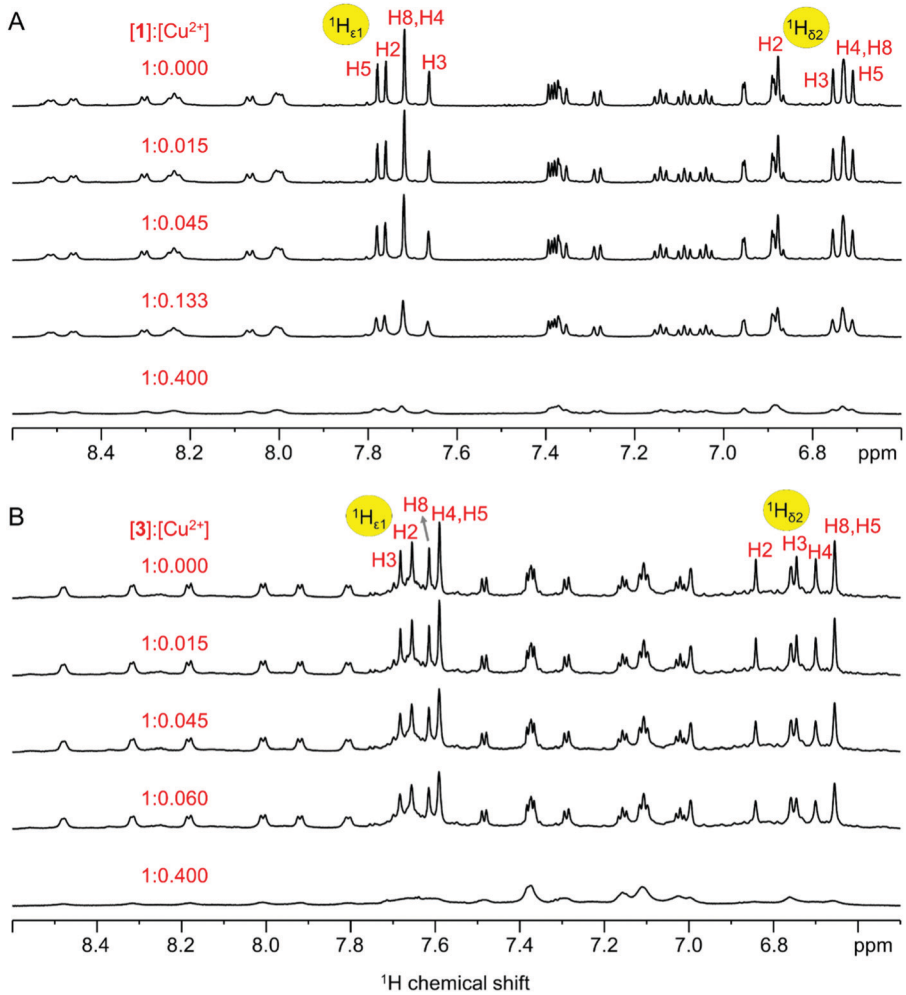

Fig. 7 1D ^{1}H NMR titration spectra of 400 μM of **1** (A) and **3** (B) with increasing amounts of Cu^{2+} in 1 : 1 DMSO-D_6/MES. Peptide : Cu^{2+} molar equivalents are indicated on each spectrum. Imidazole side chain protons were labelled with respective histidine single-letter code. For both **1** and **3**, Cu^{2+} concentration dependent reduced signal intensity of imidazole $H_{\varepsilon1}$ and $H_{\delta2}$ protons of all 5 histidines including the isolated His-8 indicate the complexation of all 5 histidines with Cu^{2+}. Therefore, a similar coordination environment is expected for both **1** and **3** with Cu^{2+}. Assuming the chelation of 2 nitrogens (on average) per Cu^{2+}, the observed stoichiometry of 1 : 2.5 cyclic peptide : Cu^{2+} is in good agreement with that observed from UV-Vis and EPR spectroscopy.

aggregation. All proton signals disappear due to paramagnetic relaxation in the presence of 0.4 equivalents of Cu^{2+}, which is well below the saturation of peptide : Cu^{2+} complex. Therefore, it is not possible to characterize the structure of Cu^{2+} mediated dimers of cyclic peptides. Since, these cyclic peptides exhibited similar binding affinity for Cu^{2+} and Zn^{2+} (MST results), we then proceeded with the characterization of N^{ε}-(2-^{13}C)acetylated-**3** (**4**, Scheme 1) complexed with Zn^{2+}, which is expected to oligomerize up to dimers only. ^{1}H NMR titration spectra of **4** were acquired in 99.95% D_2O with increasing amounts of Zn^{2+} at 303 K (Fig. 8). In the absence of Zn^{2+}, the sharp proton resonances appeared in the ^{1}H NMR spectrum of **4** are attributed to the presence of pure monomeric peptide. At 1 : 1 molar equivalents of **4** : Zn^{2+}, $H_{\varepsilon1}$ and $H_{\delta2}$ protons of imidazole ring shifted downfield and broadened indicating the chelation of all 5 histidines with Zn^{2+} and existence of monomeric and dimeric species in intermediate exchange on the NMR time scale. Even at saturation conditions *i.e.* 1 : 2.5 equivalents of **4** : Zn^{2+}, $H_{\varepsilon1}$ and $H_{\delta2}$ protons are further shifted downfield and further broadened. This is incompatible with a single conformation of the dimer, but rather suggests the presence of various dimeric arrangements (homo-stacking, hetero-stacking, and head to tail) of cyclic peptide in intermediate exchange, *i.e.* lifetimes below or around 1 ms. The observed broadening of tryptophan's aromatic ring protons and $^{13}CH_3$ doublet of Lys-1 further support the formation of Zn^{2+} mediated cyclic peptide dimers with various arrangements with different chemical shifts. We conclude that the presence of highly heterogeneous cyclic peptide/Zn^{2+} dimers hampers the formation of a specific dimer arrangement. A similar cyclic peptide dimer formation is expected in the presence of Cu^{2+} in a concentration-dependent fashion. Therefore, the observed Cu^{2+} concentration dependent diversity in the morphology of the cyclic peptide aggregates is attributed to the highly heterogeneous dimer conformations (early aggregates) of the cyclic peptide formed due to Cu^{2+} chelation.

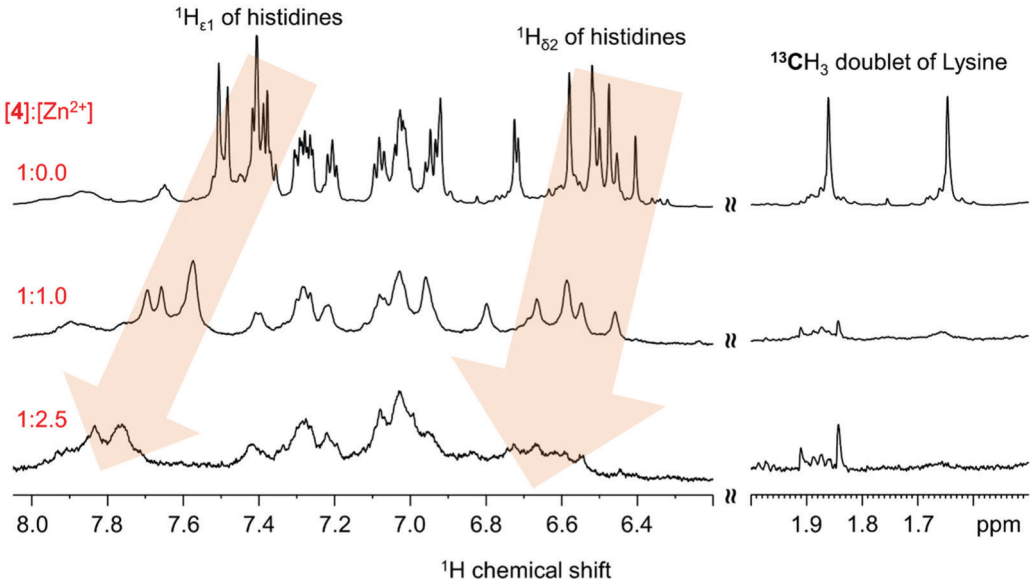

Fig. 8 Studying the effect of Zn^{2+} on cyclic peptide dimer formation. Selected regions of ^1H NMR titration spectra of **4** with increasing concentration of Zn^{2+} in 99.95% D_2O at 303 K. Peptide : Zn^{2+} molar equivalents are indicated on each spectrum. Sharp proton signals appeared in the ^1H NMR spectrum of **4** in the absence of Zn^{2+} predominantly due to the presence of pure monomeric cyclic peptide. At 1 : 1 molar equivalents of **4** : Zn^{2+}, $H_{\varepsilon1}$ and $H_{\delta2}$ protons of the histidine imidazole ring shifted downfield and broadened, indicating the chelation of all 5 histidines with Zn^{2+} and the existence of monomeric and dimeric species in intermediate-exchange on the NMR time scale. At 1 : 2.5 equivalents of **4** : Zn^{2+} (expected complete saturation of peptide : Zn^{2+} complex), $H_{\varepsilon1}$ and $H_{\delta2}$ protons of histidine imidazole ring further shifted downfield and further broadened, suggesting the presence of various dimeric arrangements (homo-stacking, hetero-stacking, and head to tail, *etc.*) in intermediate-exchange on the NMR time scale. The broadening of aromatic resonances including $^{13}CH_3$ doublet of Lys-1 further support the existence of multiple dimeric conformations of **4** in aqueous solution upon coordination with Zn^{2+}. Vertical magnification of the ^1H NMR spectra is not-to-scale.

Conclusions

Cyclic D,L-α-peptides are peptides that intrinsically self-assemble to generate cross-β-sheet tubular structures due to their even number of alternative D- and L-amino acids. Since their discovery, cyclic D,L-α-peptides have gained considerable attention due to their diverse biological activities and therapeutic potential, including antibacterial, antiviral and antiatherosclerosis activities.[54,89,90] Recently, also antiamyloidogenic activity has been reported due to structural and functional similarities of cyclic D,L-α-peptides to pathological amyloids that mediates their cross-interaction.[41–47] In contrast to natural amyloidogenic proteins, the self-assembly of cyclic peptides can be arrested at the level of the dimer by backbone *N*-methylation.[40] Thus, high dimer concentrations amenable for spectroscopic characterization can be achieved, which is exploited here for structural characterization.

In this study, we show that the histidine-rich cyclic D,L-α-peptide undergoes copper-induced self-assembly to different polymorphs, reminiscent of classical amyloids for which the effect of metal ions is controversially debated. Aggregation of the cyclic peptide strongly depends on Cu^{2+} concentration – while catalytic amounts of Cu^{2+} significantly accelerate the aggregation, higher (but still substoichiometric) concentrations of Cu^{2+} dramatically decrease the rate of formation and the amount of ThT-reactive fibrils. Moreover, Cu^{2+} concentration has a significant effect on the morphology of the self-assembled **1**. While a catalytic amount of Cu^{2+} enhances the generation of long fibrillar species, larger amounts lead to the formation of spherical aggregates. Summarizing the structural information for these aggregates, we find by EPR spectroscopy that Cu^{2+} binds to on average two histidine residues, whereas sterically coordination by 1 to 3 histidines is possible, and binding sites exhibit a significant conformational distribution. The local Cu^{2+} coordination by the dimer remains preserved in the oligomers. This suggests that the binding interface in the dimer is likely perpetuated in the oligomers and that at least part of the Cu^{2+} may act by bridging histidines from adjacent monomers. NMR spectroscopic results indicate that the dimer itself in the presence of zinc undergoes intermediate exchange on the NMR time scale between multiple conformations. This conformational ambiguity shows a reduced local order present in the cyclic peptide system from the initial interactions of the self-assembly process onwards. The structural heterogeneity is consistent with the conformational distribution of Cu^{2+} coordination observed by EPR. Hence a broadly distributed ensemble of structures is present, rather than a single structure.

Based on these results, we speculate that catalytic amounts of Cu^{2+} favour the generation of early low molecular-weight oligomers that can act as seeds to enhance the aggregation kinetics and fibrillization of the cyclic peptide. In contrast, higher concentrations of Cu^{2+} inhibit the aggregation most likely due to saturation of the available Cu^{2+} binding sites on each individual cyclic peptide molecule, which precludes coordination of multiple molecules to the same Cu^{2+} and thus inhibits stacking. These findings illustrate how very low substoichiometric amounts of Cu^{2+} may have a pronounced

influence on amyloid formation. Further, structural heterogeneity is already present at the early aggregation stage of the dimer, which may be related to polymorphism of self-assembled **1**, and is also observed for many aggregating proteins involved in neurodegeneration. The reduced order at the stage of the dimer may contribute to the mechanism of how the cross-interaction of cyclic peptides with amyloidogenic proteins suppresses fibril formation and cytotoxicity of the latter.

Materials and methods

General

All reagents for solid-phase peptide synthesis were purchased from Shanghai Hanhong Scientific (Shanghai, China) and used as received. Cyclic D,L-α-peptides **1** and **2** and the *N*-methylated derivative **3** were synthesized on 2-Cl-trityl resin and purified to homogeneity (>95% purity based on analytical HPLC) as described previously.[41,48] All peptides were dissolved in dimethylsulfoxide (DMSO) to ensure a monomeric form and the concentration of the stock solutions were determined at 280 nm based on the Trp extinction coefficient (ε_{280} = 11 000 M^{-1} cm^{-1}).

Self-assembly of the cyclic D,L-α-peptide 2

A 1:1 (v/v) solution of **2** (1 μM) in DMSO and 2-(*N*-morpholino)ethanesulfonic acid (MES; 25 mM, pH 6.6) was added to the wells of a black 96-well plate and incubated for different time intervals at room temperature with increasing concentrations of the metals (0.01–10 μM). The fluorescence of the wells was then measured at an excitation of 470 nm and emission of 500–600 nm, using a plate reader (Infinite M200, Tecan, Switzerland). Binding curves of **2** and Cu^{2+} were obtained by following changes in fluorescence intensity at 548 nm, and apparent binding affinity was calculated using GraphPad Prism (GraphPad Software, San Diego, USA) and employing a 1/1 binding model.

Thioflavin T (ThT) aggregation assay

The aggregation assay was performed in black 96-well flat-bottom plates as described previously with some modification.[43,44,91] In brief, a freshly prepared solution of **1** (400 μM) in 50% DMSO and MES (25 mM, pH 7.2) was incubated with increasing concentrations of $CuSO_4$ (in DDW) in the presence of ThT (20 μM). The plates were sealed with clear polyolefin foils and the fluorescence of bound ThT was monitored every 15 min for 72 h at 30 °C, using a plate reader (Infinite M200, Tecan, Switzerland). The plates were shaken for 1 min before each measurement. The ThT experiments were also carried out at pH 6.6 similar to other experiments, however the ThT fluorescence signal under these conditions was substantially smaller.

Dynamic light scattering (DLS) studies

Samples similar to those prepared for the fluorescent studies were also tested with dynamic light scattering (DLS, Malvern Zetasizer Nano ZS system, Malvern, UK) after different time intervals to examine the effect of Cu^{2+} on the size distribution of the self-assembled **1**.

Transmission electron microscopy (TEM) analysis

The self-assembly of **1** was also studied by TEM. Solutions of **1** in the absence or presence of Cu^{2+} were incubated for different time intervals at room temperature and then spotted onto glow-discharged, carbon-coated Formvar/copper grids (SPI supplies, West Chester, PA, USA). The samples were then blotted with a filter paper, negatively stained with 2% (w/v) uranyl acetate in water (5 μL) for 30 seconds, washed (×2) with water, blotted again, and dried. Samples were then analyzed by a Tecnai G2 TEM (FEI TecnaiTM G2, Hillsboro, Oregon, USA) operated at 120 kV.

Isothermal titration calorimetry (ITC)

All ITC measurements were carried out at 30 °C with a VP-ITC calorimeter (MicroCal Inc., Northampton, MA, USA). The titrant and sample solutions were made from the same stock buffer solution ($NaHCO_3$, 100 mM, pH 9.2) to avoid a dilution signal, and both experimental solutions were thoroughly degassed before each titration. The solution of cyclic D,L-α-peptide **1** (1 mM, 1.442 mL) in the cell was stirred at 370 rpm by the syringe to ensure rapid mixing. A solution of $CuSO_4$ (0.15 mM, 10 μL) was then delivered with an adequate interval (4 min) between injections to allow complete equilibration. A background titration, consisting of the identical titrant solution ($CuSO_4$, 0.15 mM) and the buffer solution in the sample cell, was subtracted from each experimental titration. The data were collected automatically and subsequently analyzed with the software MicroCal Origin using a two-site binding model.

Circular dichroism (CD) spectroscopy

CD measurements were carried out using a Chirascan spectrometer (Applied Photophysics, UK). Samples of **1** (10 μM) and $CuSO_4$ (10 μM) were prepared in MES buffer (10 mM, pH 6.6) and analyzed over time. Measurements were performed at room temperature in a 2 mm optical path length cell without dilution and the spectra were recorded from 260–190 nm with a step size and a bandwidth of 1 nm. The spectra are the average of three measurements after background subtraction.

Thermophoresis measurements

The association constant between **2** and the metals (Cu^{2+}, Zn^{2+}, Co^{2+}, Ni^{2+} and Fe^{3+}) was analyzed with a NanoTemper Monolith NT.115 instrument (NanoTemper Technologies GmbH, Munich, Germany), as described elsewhere.[56] In brief, a solution of **2** (10 μM) in MES (25 mM, pH 6.6) was incubated with increasing concentrations of the metals (1 μM–15 mM) and introduced to 16 MST-grade standard-treated capillaries. The measurements were carried out at room temperature and with MST power of 20% and LED Power of 70%.

EPR spectroscopy

Samples were prepared in a 1:1 mixture of DMSO:MES buffer (25 mM, pH 6.6), supplemented with the required amount of

Cu^{2+} (20 mM, in H_2O). The mixtures were incubated at room temperature in the dark and at different time intervals samples (60 μL) were filled into 3 mm (outer diameter) quartz tubes and shock frozen in liquid nitrogen for EPR measurements.

Continuous wave (cw) EPR spectra were recorded at X-band (*ca.* 9.5 GHz) on an Elexsys E580 EPR spectrometer (Bruker Biospin, Rheinstetten, Germany) equipped with a cylindrical resonator (Bruker SHQ) and an ESR900 helium flow cryostat (Oxford Instruments, Oxfordshire, UK) to stabilize the temperature at 20 K. Spectra were acquired under non-saturating conditions with a microwave power of 0.2 mW, a *B*-field modulation amplitude for lock-in detection of 0.3 mT and a conversion time of 81.92 ms using 1024 points.

The pulse EPR experiments ESEEM and HYSCORE were performed at X-band (*ca.* 9.5 GHz) using a Bruker Elexsys E580 spectrometer (Bruker Biospin, Rheinstetten, Germany) equipped with a 3 mm split-ring resonator (Bruker MS3) and cooled to 5 or 10 K employing a liquid helium flow cryostat (Oxford Instruments, Oxfordshire, UK). 3-pulse ESEEM data were acquired with the sequence $\pi/2$–τ–$\pi/2$–T–$\pi/2$–τ–echo[70] using 20 ns $\pi/2$ pulses and an interpulse delay τ of 144 ns to detect ^{14}N modulations while suppressing ^{1}H modulations. ESEEM time domain data (1024 points in 8 ns steps) were baseline corrected, using a 2nd or 4th order polynomial, apodized by a Hamming window, zero-filled to 2048 points and Fourier transformed, either with or without cross-term averaging[75] over the whole trace using the Matlab toolbox EasySpin.[92] The resulting spectra were integrated from 0 to 11 MHz to measure the ^{14}N spectral intensity, and from 13 to 16 MHz to measure the ^{1}H spectral intensity. The ratio of these two intensities was found to be proportional to the number of weakly coupled ^{14}N.[72] To quantify the relative contributions of different nuclei by integration, it is essential to integrate spectra that were Fourier transformed without cross-term averaging because cross-term averaging can lead to an imbalance in the relative contribution of different frequencies that affects linearity of the integration result. Yet, for interpretation of the ESEEM spectral shape cross-term averaging is important as it alleviates artifacts that are due to spectrometer dead time.[75]

The HYSCORE pulse sequence $\pi/2$–τ–$\pi/2$–t_1–π–t_2–$\pi/2$–τ–echo[71] was set up, using 24 ns $\pi/2$ pulses and a 16 ns π pulse through an 8 steps phase cycle. Times t_1 and t_2 were incremented independently in 16 ns steps over 400 × 400 points. The resulting 2-dimensional time domain data was baseline corrected by a 2nd or 4th order polynomial, apodized using a Hamming window, zero-filled to 1024 × 1024 points and Fourier transformed to yield the resulting 2D spectra.

EPR inter-spin distance measurements were performed at Q-band (34.5 GHz) employing the four-pulse DEER sequence[93,94] at 10 K and in 3 mm quartz tubes. DEER measurements were performed using a Q-band spectrometer equipped with a TWT amplifier with a nominal output power of 150 W and a home-built TE102 rectangular resonator.[84] Observer pulse lengths were set to 12 ns, while the pump pulse length was set to 16 ns. The pump pulse was applied at the maximum of the Cu^{2+} spectrum, the observer pulse was adjusted at a frequency offset of 100 MHz and nuclear modulations were averaged out by incrementing the first inter-pulse delay in 8 steps by 4 ns each. The data were analyzed employing the software DeerAnalysis2016.[95]

NMR spectroscopy

NMR spectra were acquired on Bruker Avance NEO 800 MHz and Bruker Avance III HD 600 MHz spectrometers equipped with 3 mm and 5 mm cryo probes, respectively. ^{1}H chemical shifts were referenced to 2,2-dimethyl-2-silapentane-5-sulfonate (DSS, δ_H 0 ppm). The chemical shift assignment of **1** and **3** was carried out using 1D ^{1}H and 2D-NOESY and TOCSY spectra acquired in a 1 : 1 mixture of DMSO-D_6 : MES buffer (25 mM, pH 6.6) at 298 K. 2D NOESY and TOCSY spectra were recorded using mixing times of 500 ms and 80 ms, respectively. ^{1}H NMR titration spectra of cyclic peptides with increasing amounts of Cu^{2+} were acquired in 1 : 1 mixture of DMSO-D_6 : MES buffer (25 mM, pH 6.6) at 298 K. ^{1}H NMR titration spectra of **4** (Scheme 1) with increasing amounts of Zn^{2+} were acquired in 99.95% D_2O at 303 K. For monitoring aggregation kinetics of **1**, cyclic peptide in 1 : 1 mixture of DMSO-D_6 : MES buffer (25 mM, pH 7.2) was incubated at 303 K in the magnet over a period of 24 h and a series of ^{1}H NMR spectra were recorded using Bruker Topspin au program multizg_vd. pH of the solution was adjusted with the aliquots of NaOH and HCl using Mettler Toledo SvenEasy S20 pH meter. A three-point calibration was done using standard buffers with pH 4, 7, 10 before measuring pH of the NMR samples. NMR spectra were processed using Topspin 3.5pl7 (Bruker, Germany).

Author contributions

D. K. and S. P. B. V. and M. R. contributed equally and wrote the manuscript with input from all authors. D. K., K. M., N. W. carried out CW EPR, HYSCORE, ESEEM, DEER, EDNMR and CHEESY-detected NMR measurements. M. S. and D. Z. performed and analyzed HR-TEM. S. P. B. V. and C. G. performed NMR experiments and analyzed the data. ITC studies were carried out and analyzed by M. A. and G. G. M. R., S. Rudnick, V. A. and M. C. performed the synthesis and chemical characterization of the cyclic D,L-α-peptides, studied their affinity to different metals, and probed the effect of the Cu^{2+} on aggregation of the cyclic D,L-α-peptides. C. G., G. J. and S. Rahimipour coordinated the project and provided guidance. All the authors revised the manuscript.

Conflicts of interest

There are no conflicts to declare.

Acknowledgements

This work was supported in part by a joint grant from German Israel Foundation (Grant No. I-1516-302.5/2019) to CG and SR. Open Access funding provided by the Max Planck Society.

References

1 C. M. Dobson, T. P. J. Knowles and M. Vendruscolo, The amyloid phenomenon and its significance in biology and medicine, *Cold Spring Harb. Perspect. Biol.*, 2020, **12**, a033878.
2 M. Goedert, R. Jakes and M. G. Spillantini, The synucleinopathies: Twenty years on, *J. Park. Dis.*, 2017, **7**, S51–S69.
3 S. H. Barage and K. D. Sonawane, Amyloid cascade hypothesis: Pathogenesis and therapeutic strategies in Alzheimer's disease, *Neuropeptides*, 2015, **52**, 1–18.
4 Y. Baradaran-Heravi, C. Van Broeckhoven and J. van der Zee, Stress granule mediated protein aggregation and underlying gene defects in the FTD-ALS spectrum, *Neurobiol. Dis.*, 2020, **134**, 104639.
5 E. Gaggelli, H. Kozlowski, D. Valensin and G. Valensin, Copper homeostasis and neurodegenerative disorders (Alzheimer's, Prion, and Parkinson's diseases and amyotrophic lateral sclerosis), *Chem. Rev.*, 2006, **106**, 1995–2044.
6 P. C. Ke, R. Zhou, L. C. Serpell, R. Riek, T. P. J. Knowles, H. A. Lashuel, E. Gazit, I. W. Hamley, T. P. Davis, M. Fändrich, D. E. Otzen, M. R. Chapman, C. M. Dobson, D. S. Eisenberg and R. Mezzenga, Half a century of amyloids: Past, present and future, *Chem. Soc. Rev.*, 2020, **49**, 5473–5509.
7 S. Ray, N. Singh, R. Kumar, K. Patel, S. Pandey, D. Datta, J. Mahato, R. Panigrahi, A. Navalkar, S. Mehra, L. Gadhe, D. Chatterjee, A. S. Sawner, S. Maiti, S. Bhatia, J. A. Gerez, A. Chowdhury, A. Kumar, R. Padinhateeri, R. Riek, G. Krishnamoorthy and S. K. Maji, α-Synuclein aggregation nucleates through liquid–liquid phase separation, *Nat. Chem.*, 2020, **12**, 705–716.
8 L. Emmanouilidis, L. Esteban-Hofer, F. F. Damberger, T. de Vries, C. K. X. Nguyen, L. F. Ibáñez, S. Mergenthal, E. Klotzsch, M. Yulikov, G. Jeschke and F. H.-T. Allain, NMR and EPR reveal a compaction of the RNA-binding protein FUS upon droplet formation, *Nat. Chem. Biol.*, 2021, **17**, 608–614.
9 C. A. McLean, R. A. Cherny, F. W. Fraser, S. J. Fuller, M. J. Smith, K. Vbeyreuther, A. I. Bush and C. L. Masters, Soluble pool of Aβ amyloid as a determinant of severity of neurodegeneration in Alzheimer's disease, *Ann. Neurol.*, 1999, **46**, 860–866.
10 J.-C. Rochet, K. A. Conway and P. T. Lansbury, Inhibition of fibrillization and accumulation of prefibrillar oligomers in mixtures of human and mouse α-synuclein, *Biochemistry*, 2000, **39**, 10619–10626.
11 R. Kayed, Common structure of soluble amyloid oligomers implies common mechanism of pathogenesis, *Science*, 2003, **300**, 486–489.
12 G. Bitan, E. A. Fradinger, S. M. Spring and D. B. Teplow, Neurotoxic protein oligomers — what you see is not always what you get, *Amyloid*, 2005, **12**, 88–95.
13 B. Winner, R. Jappelli, S. K. Maji, P. A. Desplats, L. Boyer, S. Aigner, C. Hetzer, T. Loher, M. Vilar, S. Campioni, C. Tzitzilonis, A. Soragni, S. Jessberger, H. Mira, A. Consiglio, E. Pham, E. Masliah, F. H. Gage and R. Riek, *In vivo* demonstration that α-synuclein oligomers are toxic, *Proc. Natl. Acad. Sci. U. S. A.*, 2011, **108**, 4194–4199.
14 J. M. Froula, M. Castellana-Cruz, N. M. Anabtawi, J. D. Camino, S. W. Chen, D. R. Thrasher, J. Freire, A. A. Yazdi, S. Fleming, C. M. Dobson, J. R. Kumita, N. Cremades and L. A. Volpicelli-Daley, Defining α-synuclein species responsible for Parkinson's disease phenotypes in mice, *J. Biol. Chem.*, 2019, **294**, 10392–10406.
15 G. Fusco, S. W. Chen, P. T. F. Williamson, R. Cascella, M. Perni, J. A. Jarvis, C. Cecchi, M. Vendruscolo, F. Chiti, N. Cremades, L. Ying, C. M. Dobson and A. De, Simone, Structural basis of membrane disruption and cellular toxicity by α-synuclein oligomers, *Science*, 2017, **358**, 1440–1443.
16 M. L. Giuffrida, F. Caraci, B. Pignataro, S. Cataldo, P. De Bona, V. Bruno, G. Molinaro, G. Pappalardo, A. Messina, A. Palmigiano, D. Garozzo, F. Nicoletti, E. Rizzarelli and A. Copani, β-Amyloid monomers are neuroprotective, *J. Neurosci.*, 2009, **29**, 10582–10587.
17 N. Cremades, S. W. Chen and C. M. Dobson, *International Review of Cell and Molecular Biology*, Elsevier, 2017, vol. 329, pp. 79–143.
18 M. Vivoli Vega, R. Cascella, S. W. Chen, G. Fusco, A. De Simone, C. M. Dobson, C. Cecchi and F. Chiti, The toxicity of misfolded protein oligomers is independent of their secondary structure, *ACS Chem. Biol.*, 2019, **14**, 1593–1600.
19 R. Hu, J. Diao, J. Li, Z. Tang, X. Li, J. Leitz, J. Long, J. Liu, D. Yu and Q. Zhao, Intrinsic and membrane-facilitated α-synuclein oligomerization revealed by label-free detection through solid-state nanopores, *Sci. Rep.*, 2016, **6**, 20776.
20 R. Schweitzer-Stenner, Simulated IR, isotropic and anisotropic Raman, and vibrational circular dichroism amide i band profiles of stacked β-sheets, *J. Phys. Chem. B*, 2012, **116**, 4141–4153.
21 N. V. Ilawe, R. Schweitzer-Stenner, D. DiGuiseppi and B. M. Wong, Is a cross-β-sheet structure of low molecular weight peptides necessary for the formation of fibrils and peptide hydrogels?, *Phys. Chem. Chem. Phys.*, 2018, **20**, 18158–18168.
22 S. L. Bernstein, N. F. Dupuis, N. D. Lazo, T. Wyttenbach, M. M. Condron, G. Bitan, D. B. Teplow, J.-E. Shea, B. T. Ruotolo, C. V. Robinson and M. T. Bowers, Amyloid-β protein oligomerization and the importance of tetramers and dodecamers in the aetiology of Alzheimer's disease, *Nat. Chem.*, 2009, **1**, 326–331.
23 B. Sarkar, V. S. Mithu, B. Chandra, A. Mandal, M. Chandrakesan, D. Bhowmik, P. K. Madhu and S. Maiti, Significant structural differences between transient amyloid-β oligomers and less-toxic fibrils in regions known to harbor familial Alzheimer′s mutations, *Angew. Chem., Int. Ed.*, 2014, **53**, 6888–6892.
24 B. Chandra, D. Bhowmik, B. K. Maity, K. R. Mote, D. Dhara, R. Venkatramani, S. Maiti and P. K. Madhu, Major reaction coordinates linking transient amyloid-β oligomers to fibrils measured at atomic level, *Biophys. J.*, 2017, **113**, 805–816.
25 L. Antonschmidt, R. Dervişoğlu, V. Sant, K. Tekwani Movellan, I. Mey, D. Riedel, C. Steinem, S. Becker, L. B. Andreas

and C. Griesinger, Insights into the molecular mechanism of amyloid filament formation: Segmental folding of α-synuclein on lipid membranes, *Sci. Adv.*, 2021, **7**, eabg2174.

26 M. Shahnawaz, A. Mukherjee, S. Pritzkow, N. Mendez, P. Rabadia, X. Liu, B. Hu, A. Schmeichel, W. Singer, G. Wu, A.-L. Tsai, H. Shirani, K. P. R. Nilsson, P. A. Low and C. Soto, Discriminating α-synuclein strains in Parkinson's disease and multiple system atrophy, *Nature*, 2020, **578**, 273–277.

27 A. Tiiman, J. Luo, C. Wallin, L. Olsson, J. Lindgren, J. Jarvet, R. Per, S. B. Sholts, S. Rahimipour, J. P. Abrahams, A. E. Karlström, A. Gräslund and S. K. T. S. Wärmländer, Specific binding of Cu(II) ions to amyloid-beta peptides bound to aggregation-inhibiting molecules or SDS micelles creates complexes that generate radical oxygen species, *J. Alzheimers Dis.*, 2016, **54**, 971–982.

28 Z. S. Al-Garawi, B. A. McIntosh, D. Neill-Hall, A. A. Hatimy, S. M. Sweet, M. C. Bagley and L. C. Serpell, The amyloid architecture provides a scaffold for enzyme-like catalysts, *Nanoscale*, 2017, **9**, 10773–10783.

29 J. Shearer and V. A. Szalai, The amyloid-β peptide of Alzheimer's disease binds Cu^{I} in a linear Bis-His coordination environment: Insight into a possible neuroprotective mechanism for the amyloid-β peptide, *J. Am. Chem. Soc.*, 2008, **130**, 17826–17835.

30 J. Mayes, C. Tinker-Mill, O. Kolosov, H. Zhang, B. J. Tabner and D. Allsop, β-Amyloid fibrils in alzheimer disease are not inert when bound to copper ions but can degrade hydrogen peroxide and generate reactive oxygen species, *J. Biol. Chem.*, 2014, **289**, 12052–12062.

31 J. Greenwald, W. Kwiatkowski and R. Riek, Peptide amyloids in the origin of life, *J. Mol. Biol.*, 2018, **430**, 3735–3750.

32 E. N. Salgado, R. J. Radford and F. A. Tezcan, Metal-directed protein self-assembly, *Acc. Chem. Res.*, 2010, **43**, 661–672.

33 K. J. Barnham and A. I. Bush, Metals in Alzheimer's and Parkinson's diseases, *Curr. Opin. Chem. Biol.*, 2008, **12**, 222–228.

34 C. J. Sarell, S. R. Wilkinson and J. H. Viles, Substoichiometric levels of Cu^{2+} ions accelerate the kinetics of fiber formation and promote cell toxicity of amyloid-β from Alzheimer disease, *J. Biol. Chem.*, 2010, **285**, 41533–41540.

35 J. T. Pedersen, S. W. Chen, C. B. Borg, S. Ness, J. M. Bahl, N. H. H. Heegaard, C. M. Dobson, L. Hemmingsen, N. Cremades and K. Teilum, Amyloid-β and α-synuclein decrease the level of metal-catalyzed reactive oxygen species by radical scavenging and redox silencing, *J. Am. Chem. Soc.*, 2016, **138**, 3966–3969.

36 R. M. Rasia, C. W. Bertoncini, D. Marsh, W. Hoyer, D. Cherny, M. Zweckstetter, C. Griesinger, T. M. Jovin and C. O. Fernandez, Structural characterization of copper(II) binding to -synuclein: Insights into the bioinorganic chemistry of Parkinson's disease, *Proc. Natl. Acad. Sci. U. S. A.*, 2005, **102**, 4294–4299.

37 R. A. Hauser-Davis, L. V. de Freitas, D. S. Cukierman, W. S. Cruz, M. C. Miotto, J. Landeira-Fernandez, A. A. Valiente-Gabioud, C. O. Fernández and N. A. Rey, Disruption of zinc and copper interactions with Aβ(1–40) by a non-toxic, isoniazid-derived, hydrazone: A novel biometal homeostasis restoring agent in Alzheimer's disease therapy?, *Metallomics*, 2015, **7**, 743–747.

38 N. González, T. Arcos-López, A. König, L. Quintanar, M. M. Márquez, T. F. Outeiro and C. O. Fernández, Effects of alpha-synuclein post-translational modifications on metal binding, *J. Neurochem.*, 2019, **150**, 507–521.

39 M. R. Ghadiri, J. R. Granja, R. A. Milligan, D. E. McRee and N. Khazanovich, Self-assembling organic nanotubes based on a cyclic peptide architecture, *Nature*, 1993, **366**, 324–327.

40 M. R. Ghadiri, K. Kobayashi, J. R. Granja, R. K. Chadha and D. E. McRee, The structural and thermodynamic basis for the formation of self-assembled peptide nanotubes, *Angew. Chem., Int. Ed. Engl.*, 1995, **34**, 93–95.

41 M. Richman, S. Wilk, M. Chemerovski, S. K. T. S. Wärmländer, A. Wahlström, A. Gräslund and S. Rahimipour, *In vitro* and mechanistic studies of an antiamyloidogenic self-assembled cyclic D,L-α-peptide architecture, *J. Am. Chem. Soc.*, 2013, **135**, 3474–3484.

42 M. Chemerovski-Glikman, M. Richman and S. Rahimipour, Structure-based study of antiamyloidogenic cyclic d,l-α-peptides, *Tetrahedron*, 2014, **70**, 7639–7644.

43 M. Chemerovski-Glikman, E. Rozentur-Shkop, M. Richman, A. Grupi, A. Getler, H. Y. Cohen, H. Shaked, C. Wallin, S. K. T. S. Wärmländer, E. Haas, A. Gräslund, J. H. Chill and S. Rahimipour, Self-assembled cyclic D,L-α-peptides as generic conformational inhibitors of the α-synuclein aggregation and toxicity: *In vitro* and mechanistic studies, *Chem. – Eur. J.*, 2016, **22**, 14236–14246.

44 A. Belostozky, M. Richman, E. Lisniansky, A. Tovchygrechko, J. H. Chill and S. Rahimipour, Inhibition of tau-derived hexapeptide aggregation and toxicity by a self-assembled cyclic D,L-α-peptide conformational inhibitor, *Chem. Commun.*, 2018, **54**, 5980–5983.

45 Q. Zhang, X. Hu, W. Wang and Z. Yuan, Study of a bifunctional Aβ aggregation inhibitor with the abilities of antiamyloid-β and copper chelation, *Biomacromolecules*, 2016, **17**, 661–668.

46 A. Abelein, A. Gräslund and J. Danielsson, Zinc as chaperone-mimicking agent for retardation of amyloid β peptide fibril formation, *Proc. Natl. Acad. Sci. U. S. A.*, 2015, **112**, 5407–5412.

47 J. T. Pedersen, J. Østergaard, N. Rozlosnik, B. Gammelgaard and N. H. H. Heegaard, Cu(II) mediates kinetically distinct, non-amyloidogenic aggregation of amyloid-β peptides, *J. Biol. Chem.*, 2011, **286**, 26952–26963.

48 R. Shapira, S. Rudnick, B. Daniel, O. Viskind, V. Aisha, M. Richman, K. R. Ayasolla, A. Perelman, J. H. Chill, A. Gruzman and S. Rahimipour, Multifunctional cyclic D,L-α-peptide architectures stimulate non-insulin dependent glucose uptake in skeletal muscle cells and protect them against oxidative stress, *J. Med. Chem.*, 2013, **56**, 6709–6718.

49 Z. Lengyel, C. M. Rufo, Y. S. Moroz, O. V. Makhlynets and I. V. Korendovych, Copper-containing catalytic amyloids promote phosphoester hydrolysis and tandem reactions, *ACS Catal.*, 2018, **8**, 59–62.

50 K. Zou, J.-S. Gong, K. Yanagisawa and M. Michikawa, A novel function of monomeric amyloid β-protein serving as an antioxidant molecule against metal-induced oxidative damage, *J. Neurosci.*, 2002, **22**, 4833–4841.
51 J. Chatterjee, B. Laufer and H. Kessler, Synthesis of N-methylated cyclic peptides, *Nat. Protoc.*, 2012, **7**, 432–444.
52 C. C. Curtain, F. Ali, I. Volitakis, R. A. Cherny, R. S. Norton, K. Beyreuther, C. J. Barrow, C. L. Masters, A. I. Bush and K. J. Barnham, Alzheimer's disease amyloid-β binds copper and zinc to generate an allosterically ordered membrane-penetrating structure containing superoxide dismutase-like subunits, *J. Biol. Chem.*, 2001, **276**, 20466–20473.
53 J. Danielsson, R. Pierattelli, L. Banci and A. Gräslund, High-resolution NMR studies of the zinc-binding site of the Alzheimer's amyloid β-peptide: Zinc-binding site of the amyloid β-peptide, *FEBS J.*, 2007, **274**, 46–59.
54 S. Fernandez-Lopez, H.-S. Kim, E. C. Choi, M. Delgado, J. R. Granja, A. Khasanov, K. Kraehenbuehl, G. Long, D. A. Weinberger, K. M. Wilcoxen and M. R. Ghadiri, Antibacterial agents based on the cyclic D,L-α-peptide architecture, *Nature*, 2001, **412**, 452–455.
55 D. Hoekstra, Fluorescence method for measuring the kinetics of calcium ion-induced phase separations in phosphatidylserine-containing lipid vesicles, *Biochemistry*, 1982, **21**, 1055–1061.
56 Y. Xie, X. Zhu, Y. Li and C. Wang, Analysis of the pH-dependent Fe(III) ion chelating activity of anthocyanin extracted from black soybean [*Glycine max* (L.) Merr.] coats, *J. Agric. Food Chem.*, 2018, **66**, 1131–1139.
57 C. J. Wienken, P. Baaske, U. Rothbauer, D. Braun and S. Duhr, Protein-binding assays in biological liquids using microscale thermophoresis, *Nat. Commun.*, 2010, **1**, 100.
58 M. Asmari, R. Ratih, H. A. Alhazmi and S. El Deeb, Thermophoresis for characterizing biomolecular interaction, *Methods*, 2018, **146**, 107–119.
59 A. K. Sharma, S. T. Pavlova, J. Kim, J. Kim and L. M. Mirica, The effect of Cu^{2+} and Zn^{2+} on the Aβ42 peptide aggregation and cellular toxicity, *Metallomics*, 2013, **5**, 1529.
60 D. E. Wilcox, Isothermal titration calorimetry of metal ions binding to proteins: An overview of recent studies, *Inorg. Chim. Acta*, 2008, **361**, 857–867.
61 R. J. Brea, M. E. Vázquez, M. Mosquera, L. Castedo and J. R. Granja, Controlling multiple fluorescent signal output in cyclic peptide-based supramolecular systems, *J. Am. Chem. Soc.*, 2007, **129**, 1653–1657.
62 P. K. Ajikumar, R. Lakshminarayanan, B. T. Ong, S. Valiyaveettil and R. M. Kini, Eggshell matrix protein mimics: Designer peptides to induce the nucleation of calcite crystal aggregates in solution, *Biomacromolecules*, 2003, **4**, 1321–1326.
63 D. Mandal, R. K. Tiwari, A. Nasrolahi Shirazi, D. Oh, G. Ye, A. Banerjee, A. Yadav and K. Parang, Self-assembled surfactant cyclic peptide nanostructures as stabilizing agents, *Soft Matter*, 2013, **9**, 9465.
64 M. M. Pires, D. E. Przybyla, C. M. Rubert Pérez and J. Chmielewski, Metal-mediated tandem coassembly of collagen peptides into banded microstructures, *J. Am. Chem. Soc.*, 2011, **133**, 14469–14471.
65 R. A. Cherny, J. T. Legg, C. A. McLean, D. P. Fairlie, X. Huang, C. S. Atwood, K. Beyreuther, R. E. Tanzi, C. L. Masters and A. I. Bush, Aqueous dissolution of Alzheimer's disease Aβ amyloid deposits by biometal depletion, *J. Biol. Chem.*, 1999, **274**, 23223–23228.
66 S. S. Hindo, A. M. Mancino, J. J. Braymer, Y. Liu, S. Vivekanandan, A. Ramamoorthy and M. H. Lim, Small molecule modulators of copper-induced Aβ aggregation, *J. Am. Chem. Soc.*, 2009, **131**, 16663–16665.
67 H. Liu, J. J. Schmidt, G. D. Bachand, S. S. Rizk, L. L. Looger, H. W. Hellinga and C. D. Montemagno, Control of a biomolecular motor-powered nanodevice with an engineered chemical switch, *Nat. Mater.*, 2002, **1**, 173–177.
68 J. Peisach and W. E. Blumberg, Structural implications derived from the analysis of electron paramagnetic resonance spectra of natural and artificial copper proteins, *Arch. Biochem. Biophys.*, 1974, **165**, 691–708.
69 E. Aronoff-Spencer, C. S. Burns, N. I. Avdievich, G. J. Gerfen, J. Peisach, W. E. Antholine, H. L. Ball, F. E. Cohen, S. B. Prusiner and G. L. Millhauser, Identification of the Cu^{2+} binding sites in the N-terminal domain of the prion protein by EPR and CD spectroscopy, *Biochemistry*, 2000, **39**, 13760–13771.
70 L. G. Rowan, E. L. Hahn and W. B. Mims, Electron-spin-echo envelope modulation, *Phys. Rev.*, 1965, **137**, A61–A71.
71 P. Höfer, A. Grupp, H. Nebenführ and M. Mehring, Hyperfine sublevel correlation (hyscore) spectroscopy: A 2D ESR investigation of the squaric acid radical, *Chem. Phys. Lett.*, 1986, **132**, 279–282.
72 K. I. Silva, B. C. Michael, S. J. Geib and S. Saxena, ESEEM analysis of multi-histidine Cu(II)-coordination in model complexes, peptides, and amyloid-β, *J. Phys. Chem. B*, 2014, **118**, 8935–8944.
73 S. C. Drew, Probing the quaternary structure of metal-bridged peptide oligomers, *J. Inorg. Biochem.*, 2016, **158**, 30–34.
74 S. Van Doorslaer, in *eMagRes*, ed. R. K. Harris and R. L. Wasylishen, John Wiley & Sons, Ltd, Chichester, UK, 2017, pp. 51–70.
75 S. Van Doorslaer, G. A. Sierra and A. Schweiger, Dead time-dependent line distortions in absolute-value electron spin echo envelope modulation spectra, *J. Magn. Reson.*, 1999, **136**, 152–158.
76 W. B. Mims and J. Peisach, The nuclear modulation effect in electron spin echoes for complexes of Cu^{2+} and imidazole with ^{14}N and ^{15}N, *J. Chem. Phys.*, 1978, **69**, 4921–4930.
77 J. Hernández-Guzmán, L. Sun, A. K. Mehta, J. Dong, D. G. Lynn and K. Warncke, Copper(II)-bis-histidine coordination structure in a fibrillar amyloid β-peptide fragment and model complexes revealed by electron spin echo envelope modulation spectroscopy, *ChemBioChem*, 2013, **14**, 1762–1771.
78 P. Manikandan, B. Epel and D. Goldfarb, Structure of copper(II)–histidine based complexes in frozen aqueous

solutions as determined from high-field pulsed electron nuclear double resonance, *Inorg. Chem.*, 2001, **40**, 781–787.
79 R. P. Bonomo, F. Riggi and A. J. Di Bilio, EPR reinvestigation of the copper(II)-imidazole system, *Inorg. Chem.*, 1988, **27**, 2510–2512.
80 A. Volkov, C. Dockter, T. Bund, H. Paulsen and G. Jeschke, Pulsed EPR determination of water accessibility to spin-labeled amino acid residues in LHCIIb, *Biophys. J.*, 2009, **96**, 1124–1141.
81 C. S. Burns, E. Aronoff-Spencer, G. Legname, S. B. Prusiner, W. E. Antholine, G. J. Gerfen, J. Peisach and G. L. Millhauser, Copper coordination in the full-length, recombinant prion protein, *Biochemistry*, 2003, **42**, 6794–6803.
82 C. S. Burns, E. Aronoff-Spencer, C. M. Dunham, P. Lario, N. I. Avdievich, W. E. Antholine, M. M. Olmstead, A. Vrielink, G. J. Gerfen, J. Peisach, W. G. Scott and G. L. Millhauser, Molecular features of the copper binding sites in the octarepeat domain of the prion protein, *Biochemistry*, 2002, **41**, 3991–4001.
83 N. Wili and G. Jeschke, Chirp echo Fourier transform EPR-detected NMR, *J. Magn. Reson.*, 2018, **289**, 26–34.
84 Y. Polyhach, E. Bordignon, R. Tschaggelar, S. Gandra, A. Godt and G. Jeschke, High sensitivity and versatility of the DEER experiment on nitroxide radical pairs at Q-band frequencies, *Phys. Chem. Chem. Phys.*, 2012, **14**, 10762.
85 F. D. Breitgoff, K. Keller, M. Qi, D. Klose, M. Yulikov, A. Godt and G. Jeschke, UWB DEER and RIDME distance measurements in Cu(II)–Cu(II) spin pairs, *J. Magn. Reson.*, 2019, **308**, 106560.
86 I. M. C. van Amsterdam, M. Ubbink, G. W. Canters and M. Huber, Measurement of a Cu–Cu distance of 26Å by a pulsed EPR method, *Angew. Chem., Int. Ed.*, 2003, **42**, 62–64.
87 T. F. Cunningham, M. R. Putterman, A. Desai, W. S. Horne and S. Saxena, The double-histidine Cu^{2+}-binding motif: A highly rigid, site-specific spin probe for electron spin resonance distance measurements, *Angew. Chem., Int. Ed.*, 2015, **54**, 6330–6334.
88 T. F. Cunningham, M. D. Shannon, M. R. Putterman, R. J. Arachchige, I. Sengupta, M. Gao, C. P. Jaroniec and S. Saxena, Cysteine-specific Cu^{2+} chelating tags used as paramagnetic probes in double electron electron resonance, *J. Phys. Chem. B*, 2015, **119**, 2839–2843.
89 W. S. Horne, C. M. Wiethoff, C. Cui, K. M. Wilcoxen, M. Amorin, M. R. Ghadiri and G. R. Nemerow, Antiviral cyclic d,l-α-peptides: Targeting a general biochemical pathway in virus infections, *Bioorg. Med. Chem.*, 2005, **13**, 5145–5153.
90 Y. Zhao, L. J. Leman, D. J. Search, R. A. Garcia, D. A. Gordon, B. E. Maryanoff and M. R. Ghadiri, Self-assembling cyclic d, l -α-peptides as modulators of plasma HDL function. a supramolecular approach toward antiatherosclerotic agents, *ACS Cent. Sci.*, 2017, **3**, 639–646.
91 G. Leshem, M. Richman, E. Lisniansky, M. Antman-Passig, M. Habashi, A. Gräslund, S. K. T. S. Wärmländer and S. Rahimipour, Photoactive chlorin e6 is a multifunctional modulator of amyloid-β aggregation and toxicity *via* specific interactions with its histidine residues, *Chem. Sci.*, 2019, **10**, 208–217.
92 S. Stoll and A. Schweiger, EasySpin, a comprehensive software package for spectral simulation and analysis in EPR, *J. Magn. Reson.*, 2006, **178**, 42–55.
93 R. E. Martin, M. Pannier, F. Diederich, V. Gramlich, M. Hubrich and H. W. Spiess, Determination of end-to-end distances in a series of TEMPO diradicals of up to 2.8 nm length with a new four-pulse double electron electron resonance experiment, *Angew. Chem., Int. Ed.*, 1998, **37**, 2833–2837.
94 M. Pannier, S. Veit, A. Godt, G. Jeschke and H. W. Spiess, Dead-time free measurement of dipole–dipole interactions between electron spins, *J. Magn. Reson.*, 2000, **142**, 331–340.
95 G. Jeschke, V. Chechik, P. Ionita, A. Godt, H. Zimmermann, J. Banham, C. R. Timmel, D. Hilger and H. Jung, DeerAnalysis2006—a comprehensive software package for analyzing pulsed ELDOR data, *Appl. Magn. Reson.*, 2006, **30**, 473–498.